AIMS Geosciences

AIMS Geosciences, 11(4): 946–978.
DOI: 10.3934/geosci.2025041
Received: 01 March 2025
Revised: 26 August 2025
Accepted: 26 September 2025
Published: 17 November 2025

https://www.aimspress.com/journal/geosciences

Research article

Highway construction at Kvithammar-Åsen, mid-Norway: Geotechnical characterization of very sensitive clay deposits

Anders Lindgård, Vidar Gjelsvik*, Åse Marit Wist Amdal, Sølve Hov, Jean-Sébastien L'Heureux, Katharina Kahrs and Sigbjørn Rønning

Norwegian Geotechnical Institute, Trondheim, Norway

* **Correspondence:** Email: vidar.gjelsvik@ngi.no; Tel: +47 932 80 361.

Abstract: The properties of vast, sensitive clay deposits have been investigated for the construction of the E6 Kvithammar-Åsen highway, north of Trondheim, in mid-Norway. Highway construction included the design of up to 14 m thick road embankments, made possible by stabilization works using lime-cement and vertical drains. Airborne electromagnetic scanning was performed to optimize the field investigation program, which included a large number of total and rotary pressure soundings, CPTU, piezometers, and undisturbed sampling. Advanced laboratory testing was performed to characterize the engineering properties of the clay (i.e., strength, stiffness, and hydraulic properties). In this paper, the properties of the clay deposits were compared to reference data from multiple sites in Norway. The laboratory results indicated that sample disturbance is a key uncertainty, affecting the interpretation of both strength and stiffness parameters. The undrained shear strength ranged approximately from 20 to 120 kPa. The friction angle, interpreted from undrained triaxial tests, was approximately 30°–33°. The overconsolidation ratio ranged from 1 to 6, depending mainly on depth. A correlation with the least scatter for the stiffness parameters was found between the modulus in the overconsolidated range (M_0) and the preconsolidation stress (σ_p'). For samples of quality 1, the average ratio of M_0/σ_p' was 33. In addition, some results from large-scale testing of lime-cement stabilization and road embankments on soft ground are presented. For lime-cement-stabilized clay, the ratio of passive to active maximum shear strength was between 0.45 and 0.95, with an average of 0.67. This ratio is crucial in design. Settlement predictions from the design phase for road embankments on soft soil at Holan agreed with measured values during construction.

Keywords: site characterization; sensitive clay; highway construction; large-scale field tests

1. Introduction

E6 Kvithammar-Åsen is a highway construction project close to Trondheim in mid-Norway. The public project owner, Nye Veier, is constructing a 19 km four-lane highway with the help of the contractor Hæhre Entreprenør. Geotechnical expertise is being provided by the Norwegian Geotechnical Institute (NGI), by a group of engineers led by Aas-Jakobsen Trondheim. Approximately 7 km of the road is being built on challenging soil conditions, with vast areas of sensitive marine clays. Such deposits are present in the lowland area of mid-Norway and have been the locus of catastrophic landslides over time. Some of the major landslides in mid-Norway included Kattmarka [1], Rissa [2], and Esp [3].

The most important geotechnical engineering problems encountered by this project included stability and settlements of road embankments, foundation design for bridges, and the stability of quick clay slopes and cuts. Solutions to the stability issues included topographic adjustments, lime-cement stabilization of clay, embankments of light fill aggregate, and installation of vertical drains. The vertical drains also address the issue of settlements of road embankments, together with lime-cement stabilization and preloading.

The objectives of this paper are to summarize the laboratory work and field investigations and provide examples of large-scale tests (i.e., embankment tests and lime-cement soil stabilization) performed during the design and construction stages of the E6 Kvithammar-Åsen project. A comprehensive dataset was key for selecting reliable and sustainable foundation solutions in this challenging area [4]. The results presented herein form a useful reference for geotechnical engineers working on the design of foundation solutions in soft and sensitive clay deposits worldwide.

Critical infrastructure developments, like highways and railways, cover large areas with complex geotechnical challenges. Challenges include difficult ground conditions such as soft clays, silt and loose sands, and regions historically prone to landslides. Characterization of such areas is mandatory [5,6], aiming to set a benchmark for safe and sustainable road construction.

2. Regional settings and site location

The project area is located approximately 30 km northeast of Trondheim in mid-Norway. In this paper, only the portion of the Kvithammar-Åsen E6 highway being constructed in the municipality of Stjørdal will be presented (Figure 1). As illustrated in Figure 1, the road is being constructed on thick marine deposits in two zones: Holan and Langsteindalen Valley. The marine sediments emerged from the sea following a fall in the relative sea-level around the Trondheimsfjorden region during the Holocene period. Following their emergence, clay deposits were subjected to percolating fresh groundwater flow, which eventually led to leaching of the clays. Hence, very sensitive and quick clay is locally found in the study area.

In the area of Holan, the large river Vollselva and its tributaries have eroded ravines in the marine deposits. Landslide scars are visible in the terrain and identified on the Quaternary geology maps. The

highway is being constructed in terrain approximately 20–50 meters above sea-level (MASL). In the area of Langsteindalen Valley, there are no observations of ravines or landslide scars. Terrain elevation is approximately 100–120 MASL.

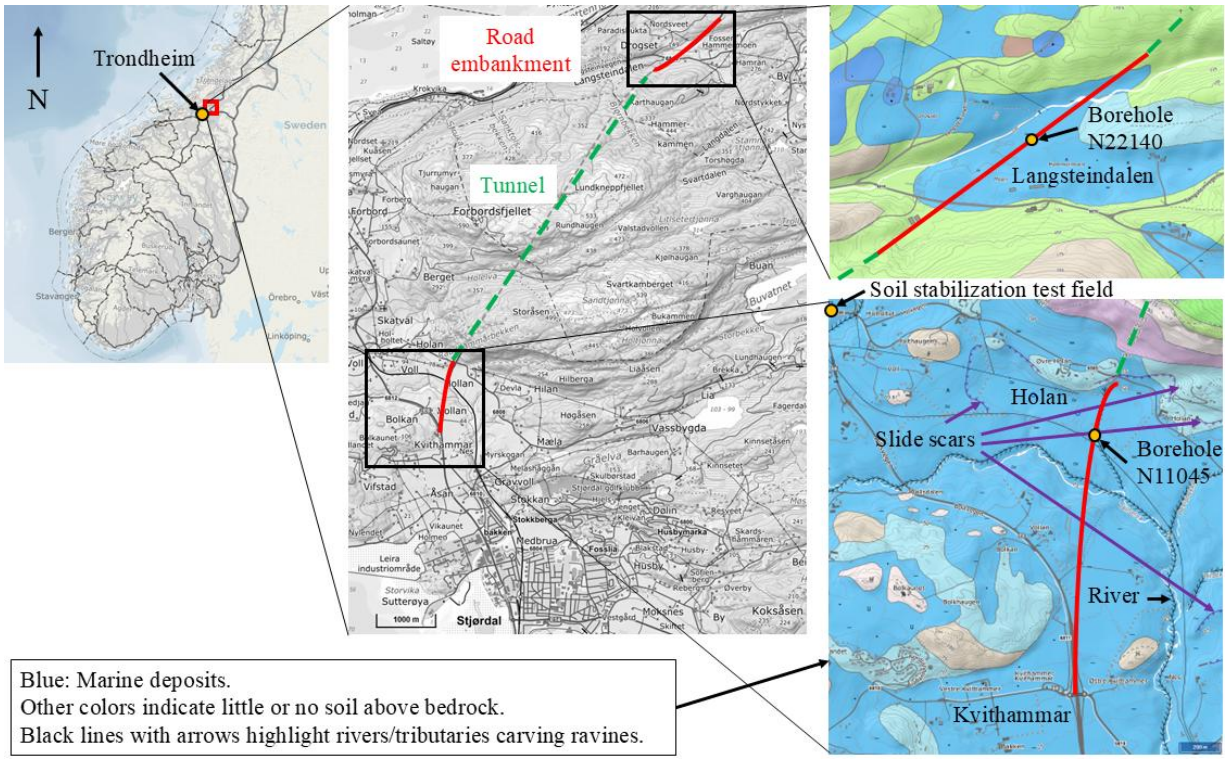

Figure 1. Left and center: Site location and location of highway. Right: Quaternary geology, borehole locations, and soil stabilization test field at Langsteindalen (upper right) and Holan area (bottom right). Maps from [7] and [8].

3. Field and laboratory investigations

To characterize a relatively large area as efficiently as possible, an investigation strategy involving airborne electromagnetic (AEM) scanning was adopted [9]. AEM geoscanning was performed at an early stage of the project. The main delivery was a map showing the depth to bedrock. The bedrock model was calibrated with geotechnical soundings available from earlier design stages of the highway construction project. The accuracy of the model was later updated with new soundings. Even though AEM geoscanning gives less reliable depth to bedrock than soundings, this method can cover large areas efficiently. This allowed the engineers to prioritize and narrow down the areas that needed thorough investigations, thereby resulting in fewer soundings and a shorter period of field work.

After completing the AEM work, total soundings were the preferred in situ method to map the depth to bedrock and soil layering. Total soundings are performed with a drill bit that is rotated and pushed into the soil. Flushing with water or air, increased speed of rotation and hammer drilling can be used to keep the penetration rate constant. The normal procedure is to drill 3 m into the bedrock [10].

Rotary pressure soundings are not able to penetrate bedrock, since the equipment does not have

a drill bit and options for flushing and hammer drilling [11]. However, they are more efficient than total soundings. This is especially true during winter, when freezing water may cause trouble with total soundings. Rotary pressure soundings were performed to map soil layering and depth to bedrock or other non-penetrable layer. Soundings may indicate the presence of quick clay, but identification can only be confirmed by laboratory tests on samples.

Cone penetration tests (CPTU) can be performed relatively efficiently and give more precise information about soil layering [12]. Using correlations, parameters for strength and stiffness can be estimated. In this project, CPTU soundings were often performed in combination with total soundings or rotary pressure soundings to efficiently gain information.

Sampling and installation of vibrating wire pore-pressure measurements were also carried out, but to a lesser extent than the soundings. Laboratory testing on the retrieved samples and information from pore-pressure measurements were directly used in CPTU interpretation, stability calculations, and settlement calculations. Field and laboratory investigations carried out on the E6 project in Stjørdal municipality are thoroughly described in [13]. A summary is given in Tables 1 and 2.

Two separate areas will be presented in more detail in this paper: Holan and Langsteindalen Valley. In both cases, extensive laboratory and in situ geotechnical testing has been carried out to supplement the full-scale testing, as follows:

- Holan: Data from borehole location N11045 is presented in this article. It includes data from both piston (72 mm) and mini-block (160 mm) sampling. The clay at this location has low-to-medium sensitivity. Large-scale field tests at this location include full scale embankment and soil stabilization test field.
- Langsteindalen Valley: Data from borehole location N22140 provides a good representation of the soil in this area. Samples were collected using the Sherbrooke mini-block (160 mm) sampler. Large-scale field testing included a full-scale embankment.

Table 1. Summary of field investigations.

Field investigations	Number of locations
Airborne electromagnetic (AEM) scanning [9]	Whole site
Total soundings [10]	202
Rotary pressure soundings [11]	147
Cone penetration tests (some with resistivity and seismic modules) [14]	101
Vibrating wire piezometers [15]	29
Fixed piston sampling (54 mm and 72/75 mm) [16]	42
Mini-block sampling (160 mm) [17]	2
Auger sampling (bag) [16]	10

4. Engineering geology

4.1. Depositional environment

The sediments in the study area were deposited in a fjord marine environment following the retreat of the glaciers in the Kvithammar-Åsen region approximately 12,000–13,000 years ago [18]. During

the Holocene, the region was subjected to a relative fall of the sea level, and fjord-marine sediments emerged from the sea. Today, the marine limit in the study area is situated at about 175 m above present-day sea level. The depositional environment is expected to be similar to that of other well know test sites on marine clays around Trondheim, including Klett [5] and Tiller-Flotten [19].

Table 2. Summary of laboratory testing methods.

Laboratory test methods	Number of tests
Water content analysis	Ca. 550
Bulk density	Ca. 250
Fall cone tests	Ca. 500
Unconfined compression tests	Ca. 200
Atterberg limits	Ca. 200
Grain size distribution	35
Triaxial tests (anisotropically consolidated undrained compression tests, CAUC)	65
Triaxial tests (anisotropically consolidated undrained extension tests, CAUE)	3
Direct simple shear tests (DSS)	5
Oedometer tests (constant rate of strain, CRS)	68
Oedometer tests (incremental loading, IL)	4
Tests on lime-cement-stabilized clay	20

4.2. Post-depositional processes

As the clay emerged from the sea, it was exposed to leaching from fresh groundwater flow. Fresh water percolating downward through the marine deposits removed the salt ions and left behind a metastable, sensitive structure made up of flocculated clay minerals. The high sensitivity of Norwegian quick clays is usually attributed to the leaching by fresh groundwater of the salts within the grain structure [20].

Once above sea level, subaerial exposure has produced a weathered crust. This crust is close to the soil surface and, through weathering, drying, and cracking, has changed its properties and become firm. During its emergence, the clay deposit was locally covered by coarser beach and fluvial deposits of varying thicknesses. Also, the clay deposit was locally eroded by creeks, rivers, and landslides.

4.3. Stress history

The groundwater level and pore-pressure distribution with depth vary over the characterized areas. In the Holan area, pore pressure in the relatively flat areas, including the top of ravines, is typically hydrostatic or below hydrostatic conditions, with groundwater level approximately 0–2 m below terrain. Pore-pressure profiles exceeding hydrostatic conditions are generally observed at the bottom of the ravines.

In the flat areas at the bottom of Langsteindalen Valley, hydrostatic pore-pressure conditions with the groundwater table approximately at terrain level are observed. In the sloping clay terrain toward the south of the valley, a pore-pressure distribution below hydrostatic is mainly measured. However,

conditions above hydrostatic are also measured in these slopes. This may be related to seepage from the hilly terrain surrounding the valley.

Figure 2 summarizes the interpreted overconsolidation ratio at Holan (location N11045). Except for the green line, the data fit quite well with the line assuming an aging factor of 1.2 and a current terrain elevation of 5 m below terrain level at deposition. This indicates that terrain elevation has not changed much since deposition. At the bottom of the ravines, the overconsolidation ratio is higher. This reflects the unloading that has happened due to creeks and rivers carving the ravines; see Figure 1.

Borehole N22140 is located in the flat area at the bottom of Langsteindalen Valley. Figure 3 summarizes the interpreted overconsolidation ratio. Similarly to location N11045, the data fit quite well with the line, assuming an aging factor of 1.2 and a current terrain elevation 6 m below terrain level at deposition. The oedometers classified with quality 1 and 2 suggest a slightly higher previous elevation level. In Langsteindalen Valley, there are no visible ravines or slide scars, even though a river runs through the valley. Based on this, normally consolidated clay with low OCR is expected. A previous terrain elevation of approximately 0–10 m above the current terrain elevation is interpreted from CPTU tests at the bottom of the valley. Interpretations at location N22140 also suggest that the clay is slightly overconsolidated, and this is likely due to erosion over time at the bottom of the valley.

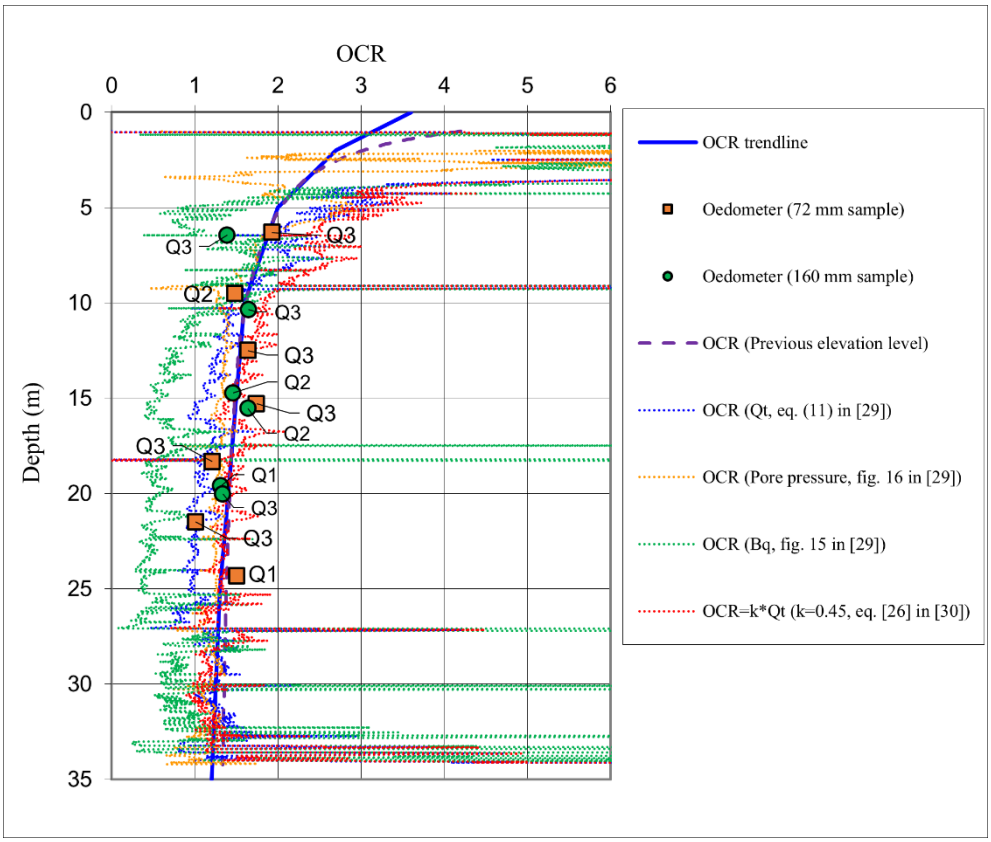

Figure 2. Overconsolidation ratio (OCR) at Holan (location N11045) interpreted from oedometer tests, CPTU correlations, and previous elevation levels (assumed 5 m above current terrain level, aging factor 1.2). Q1–Q3 refers to the oedometer test quality according to the Karlsrud and Hernandez-Martinez [21] criterion (chapter 6.1).

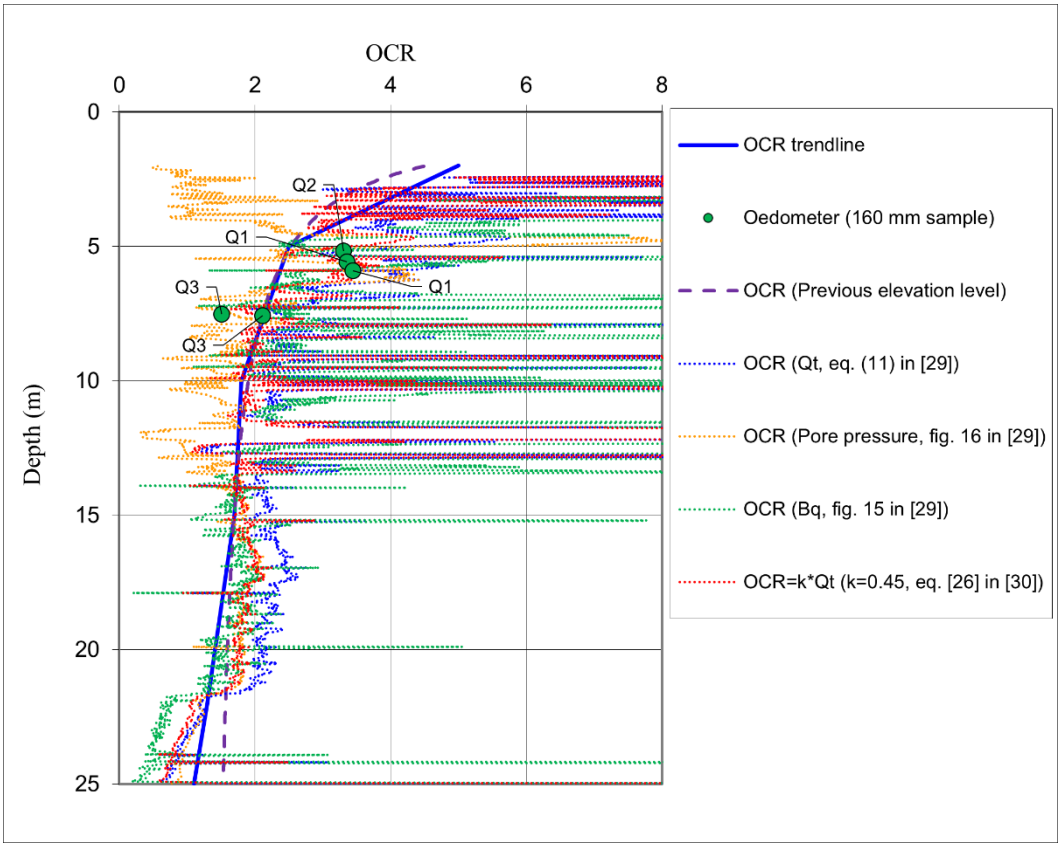

Figure 3. Overconsolidation ratio (OCR) in Langsteindalen Valley (location N22140) interpreted from oedometer tests, CPTU correlations, and previous elevation levels (assumed 6 m above current terrain level, aging factor 1.2). Q1–Q3 refers to the oedometer test quality according to the Karlsrud and Hernandez-Martinez [21] criterion (chapter 6.1).

4.4. Stratigraphy

In the Holan area, there is generally a top layer of dry crust with a thickness of approximately 0–5 m. Under the planned road in Langsteindalen Valley, the thickness of a top layer consisting of silt, sand, and gravel increases up to approximately 10 m toward northeast. Marine deposits are generally found below the top layer in the areas of Holan and Langsteindalen Valley, and these primarily consist of clay. The clay is, in some places, layered with silt and sand. The undrained strength of the clay ranges from 10 to above 50 kPa, and sensitivity ranges from below 8 to above 30. In parts of the area, a stiff and coarse unit of varying thickness, interpreted as till, was detected between the clay and the bedrock. Stratigraphy at locations N11045 (Holan) and N22140 (Langsteindalen Valley) is illustrated in Figures 4 and 5. Figure 5 also includes data from location N22109. N22109 is located 65 m northeast of N22140, and the top layer is therefore thicker than indicated in the figure.

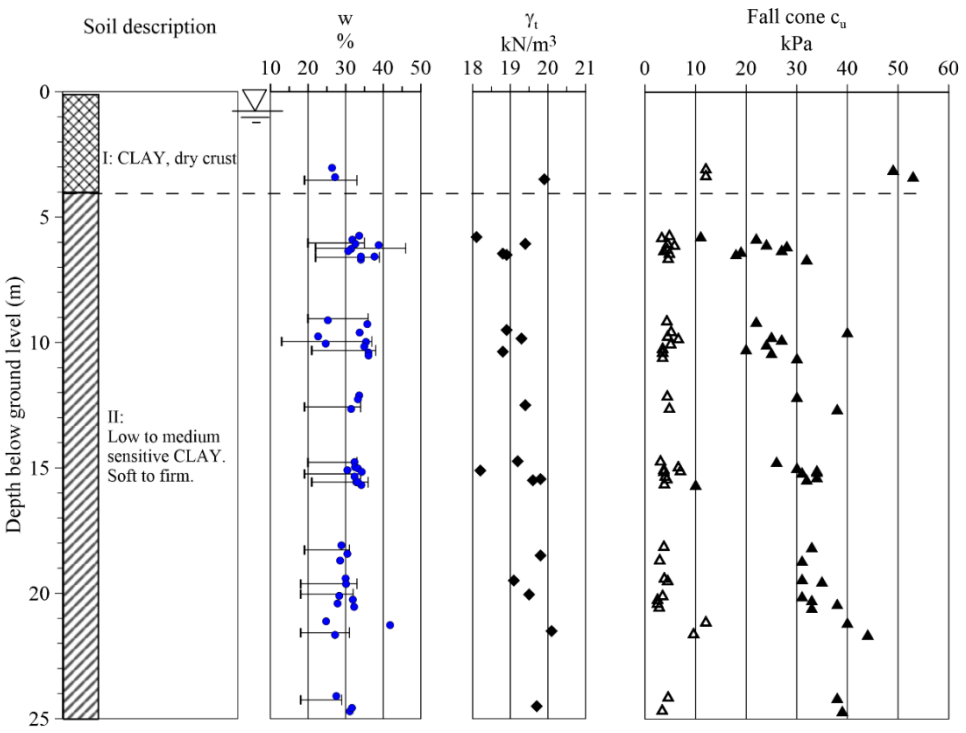

Figure 4. Soil layering, water content, and Atterberg limits, bulk density, and undrained shear strength from fall cone tests (open symbols indicate remolded strength) at location N11045 at Holan.

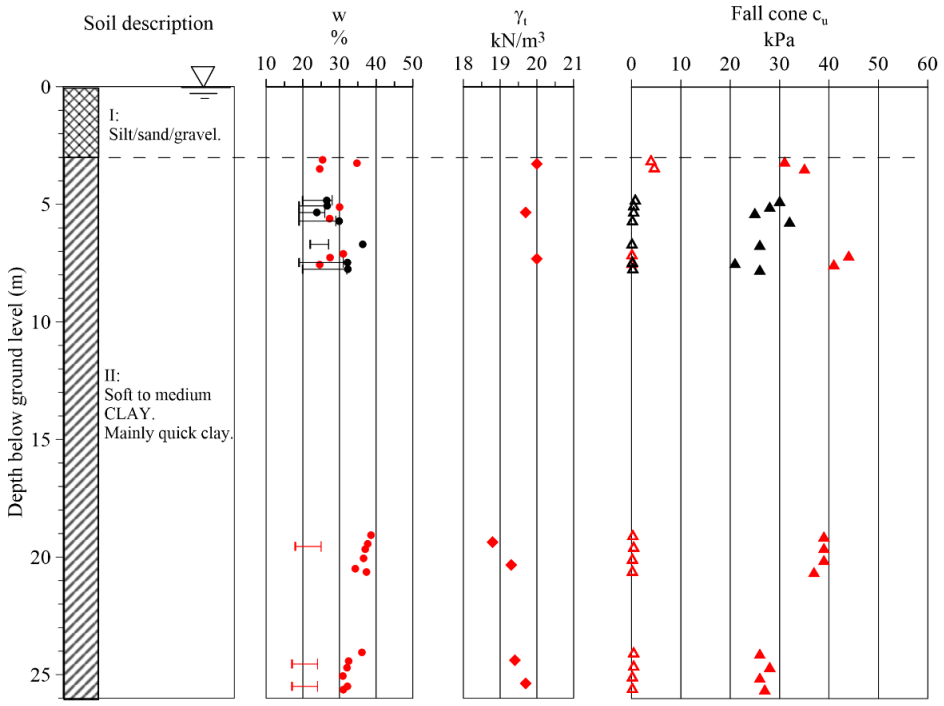

Figure 5. Soil layering, water content, and Atterberg limits, bulk density, and undrained shear strength from fall cone tests (open symbols indicate remolded strength) in Langsteindalen Valley at locations N22140 (Black) and N22109 (Red) (located 65 m northeast of N22140).

4.5. Grain size distribution

Grain size distribution was determined by the falling drop method [22]. Figure 6 shows the results from Holan (location N11045) and Langsteindalen Valley (locations N22140 and N22109). At Holan, the clay content is >35% for all tests, between 6 and 20 m depth. In Langsteindalen Valley, clay content increases with depth. When the clay content is above 30%, the material is classified as a clay, without any secondary notation of silty, sandy, etc. [23].

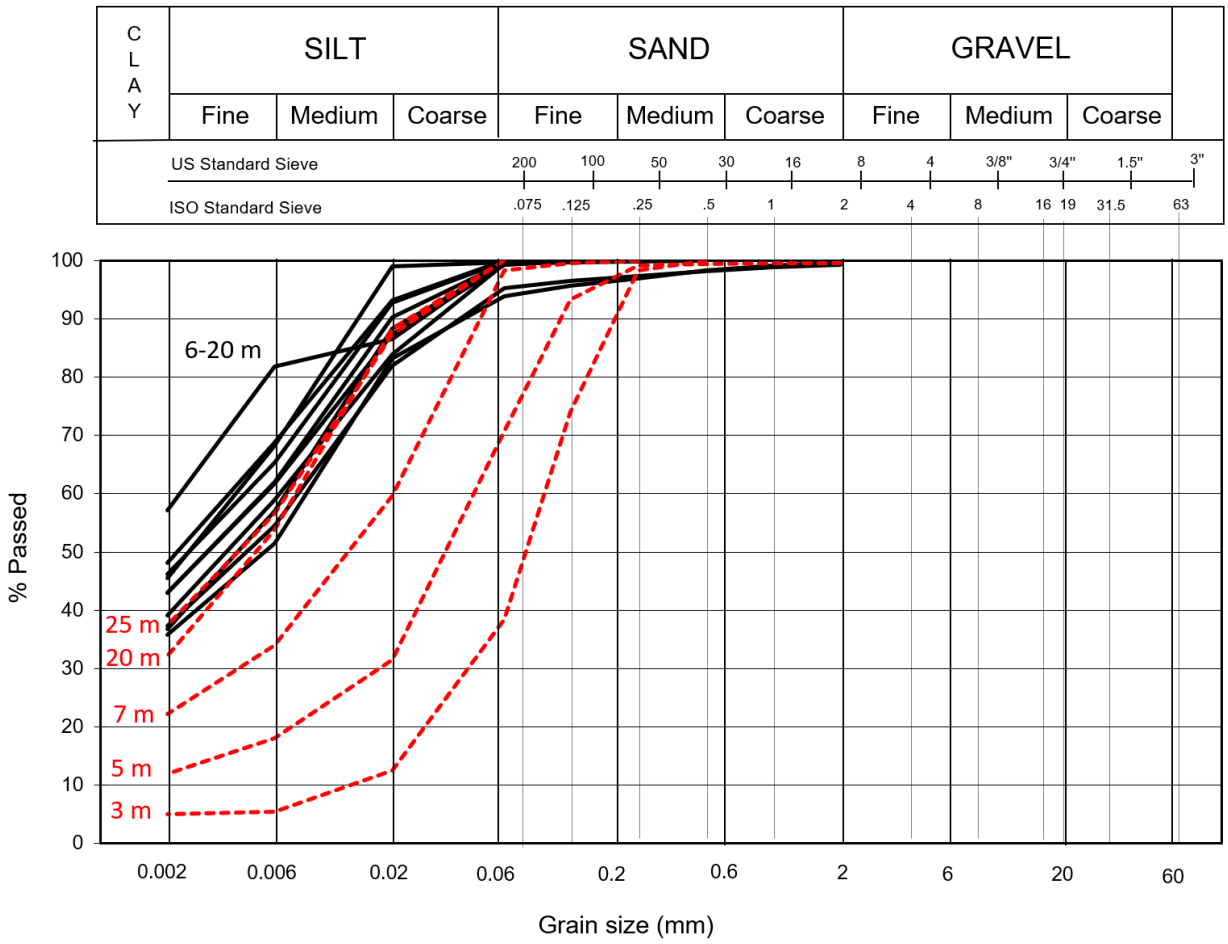

Figure 6. Grain size distribution in black for Holan (location N11045) and in red for Langsteindalen Valley (locations N22109 and N22140).

5. State and index properties

5.1. Water content

Figures 4 and 5 summarize soil layering and index properties at both Holan and Langsteindalen Valley (locations N11045 and N22140/N22109). On average, the natural water content is approximately 30%–35%. At location N11045 (Holan), a slight decrease with depth of measured water content is observed. At location N22109 (Langsteindalen Valley), the trend is opposite.

5.2. Bulk density

Bulk density is plotted in Figures 4 and 5. Typically, bulk density is in the range 19–20 kN/m^3. At location N11045 (Holan), there is a slight increase with depth of measured bulk density. The trend is opposite to the natural water content, which is as expected. At location N22109 (Langsteindalen Valley), the bulk density decreases with depth, while the natural water content increases.

5.3. Atterberg limits

Figures 4 and 5 show that the average plasticity of the clay at location N11045 (Holan) is 16%, while it is 8% at location N22140/N22109 (Langsteindalen Valley). According to the Norwegian classification system [23], the clay at locations N11045 and N22140/N22109 is classified with medium and low plasticity, respectively. Norwegian clays generally show relatively low plasticity, and therefore the limits are higher in the ISO classification system [24]. For sensitive clays, it is normal to observe natural water content higher than the liquid limit [25]. At both N11045 and N22140 locations, the natural water content is typically close to the liquid limit. Since the fall cone tests measure higher sensitivity at N22140, one would expect the difference between the natural water content and the liquid limit to be higher at this location [26]. Looking at data from the quick clay at N22109, located approximately 65 m northeast of N22140, the water content at 20–25 m depth is approximately 10% higher than the liquid limit.

5.4. Sensitivity and remolded undrained shear strength

In [23], clay sensitivity is defined as low when $S_t = c_u/c_{ur} < 8$, high when $St > 30$, and medium in between. The term "sensitive clay" in this article generally refers to clays with high sensitivity. The term "quick clay" is solely defined by the remolded undrained shear strength, being clays with $c_{ur} <$ 0.5 kPa [23], determined by the method described in [27]. Figure 5 illustrates that the clay at location N22140/N22109 (Langsteindalen Valley) is generally classified as quick clay. At location N11045 (Holan), the clay is classified as low-to-medium sensitive.

5.5. Identification of quick clay from soundings

Several field investigation methods may be used to indicate the presence of quick clay layers. However, certain identification is only possible with fall cone tests in the laboratory. A complete description of field investigations, including soundings (e.g., total soundings and CPTU) and resistivity measurements (e.g., electrical resistivity tomography (ERT) and AEM scanning) can be found in [28], [25], and [29].

In this project, the main methods used to indicate quick clay layers were total soundings, rotary pressure soundings, and CPTU. The first two methods indicate sensitive clay if the change in penetration force with depth is negative or barely increasing. There are several ways to use CPTU data to indicate quick clay. Two simple indicators are low side friction measurements and values >1 of the derived pore-pressure parameter $B_q = \Delta u/q_n$. Figure 7 shows soundings in Langsteindalen Valley (location N22140), where quick clay is present below approximately 5 m depth.

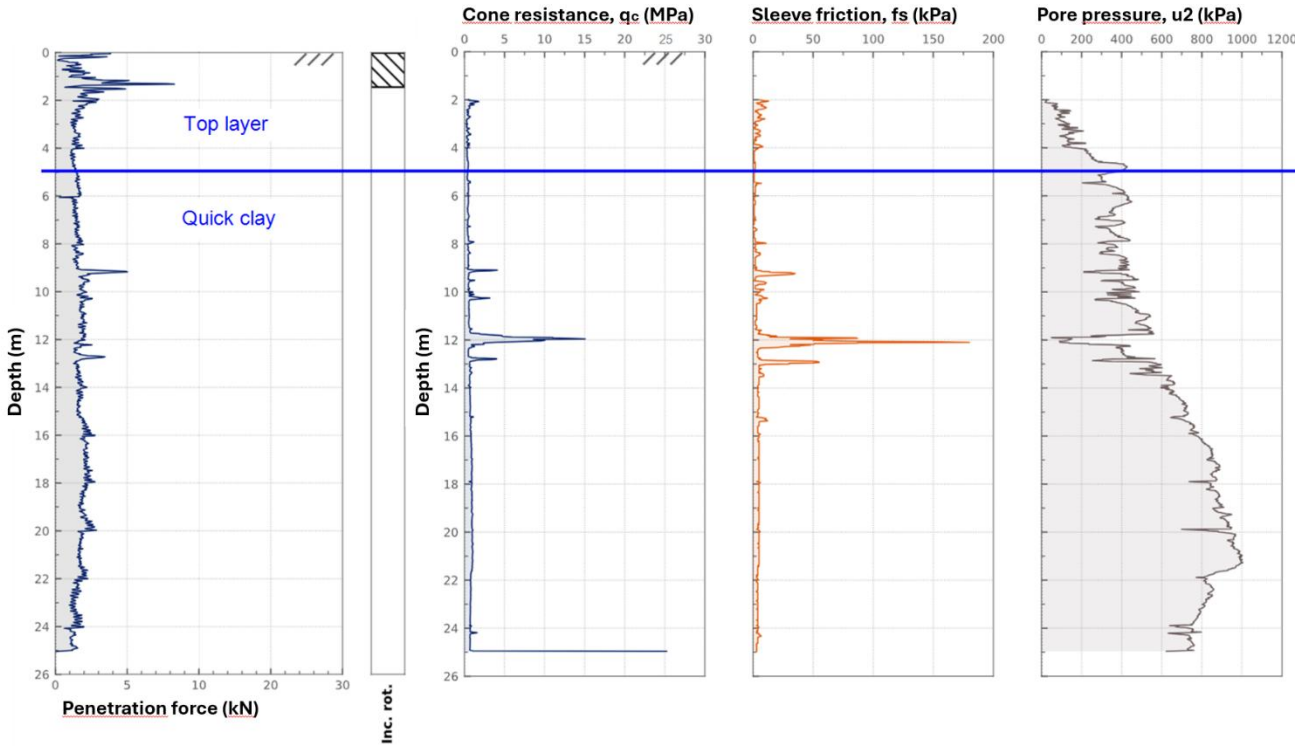

Figure 7. Rotary pressure sounding and CPTU data in Langsteindalen Valley (location N22140).

6. Engineering properties

6.1. Preconsolidation/yield stress and overconsolidation ratio

Preconsolidation/yield stress (σ_p') and overconsolidation ratio (OCR = σ_p'/p_0') were interpreted from constant rate of strain (CRS) oedometer tests. Interpretation was performed with the Karlsrud and Hernandez-Martinez method [21]. The method estimates the preconsolidation stress to be the average of the stress when the tangent modulus starts decreasing toward σ_p' and the stress when the modulus curve begins to increase along the virgin modulus line (see Figure 8). Sample quality is evaluated based on the ratio of modules M_0 and M_L. Quality 1 means very good to excellent, and quality 4 is very poor.

To support the final interpretation of the design trendline for OCR, oedometer results were compared to several CPTU correlations, as shown in Figures 2 and 3. The correlations can be found in [30] and [31]. The correlation from Paniagua et al. is adopted from [32], which states that the empirical factor k is site-specific and varies in the range 0.2–0.5. The same authors [31] found that k = 0.44 fits well at the Tiller-Flotten sensitive clay test site, just south of Trondheim [19]. A similar empirical factor k = 0.45 fits reasonably well with interpretations of the oedometer tests at locations N11045 (Holan) and N22140 (Langsteindalen Valley) (see Figures 2 and 3).

Figure 2 shows that the interpreted values of OCR, from samples of all qualities at location N11045 (Holan), plot both higher and lower than the OCR trendline. There are more samples of better quality (1 and 2) from 160 mm mini-block samples, compared to 72 mm piston samples. This aligns with previous experience [21].

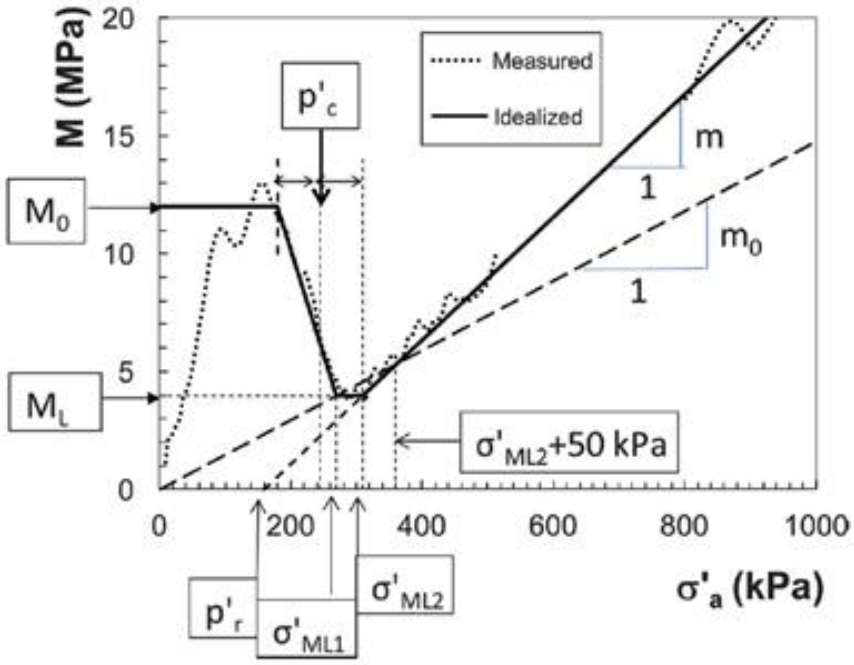

Figure 8. Interpretation of preconsolidation and stiffness parameters from the tangent modulus curve of an oedometer test. Figure from [21].

The limited amount of oedometer tests performed at location N22140 (Langsteindalen Valley) suggests that the OCR interpretations from higher quality tests are less scattered (see Figure 3).

Sample disturbance may also be classified with the Lunne criterion [33]. The number of tests that are classified as quality 1 and 2 with both the Karlsrud and Hernandez-Martinez [21] criterion and the Lunne [33] criterion was compared for the tests in this project. The total number of tests of quality 1 and 2 is approximately the same in total for both criteria, but there are fewer samples of quality 1 with the Lunne criterion. This is thought to be related to *false* deformations at the beginning of the test, until full contact is established against the oedometer ring [19,34]. Classification with the Karlsrud and Hernandez-Martinez criteria is not significantly affected by these deformations.

6.2. Stiffness from oedometer tests

Interpretation of moduli M_0 and M_L versus preconsolidation stress is shown in Figures 9 and 10. Both figures show a trend of increase in modulus with increasing preconsolidation stress. For samples of quality 1, the average ratio of M_0/σ_p' is 33. The modulus in the overconsolidated range (M_0) shows fairly good correlation with the preconsolidation stress, yielding slightly higher values for higher-quality samples. The modulus at the onset of the normally consolidated range (M_L) shows far more scatter and a larger impact of sample disturbance compared to the overconsolidated range. There is a clear trend that M_L is lower for higher-quality samples. This aligns with experience from [21].

Figure 11 shows the interpreted modulus number m versus water content. The data points from this project plot between the high and low trendlines based on tests on high-quality block samples [21]. The data is quite scattered. However, there is a trend showing that the highest-quality samples yield slightly higher values of m.

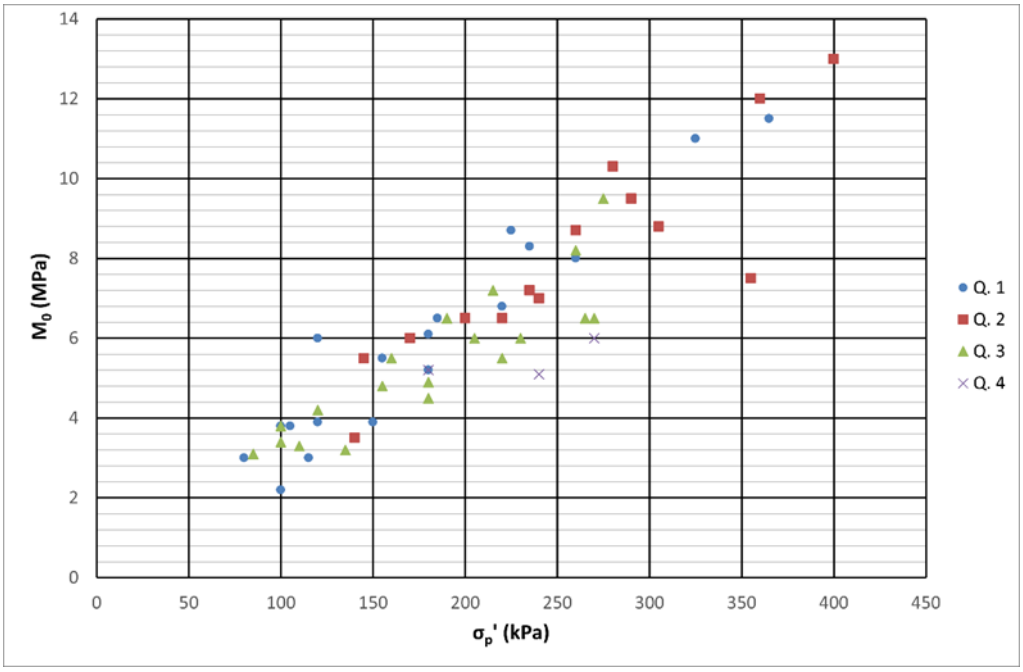

Figure 9. Interpretation of modulus M_0 versus preconsolidation stress σ_p'. Q1–4 refers to the oedometer test quality according to the Karlsrud and Hernandez-Martinez [21] criterion. Figure adapted from [4].

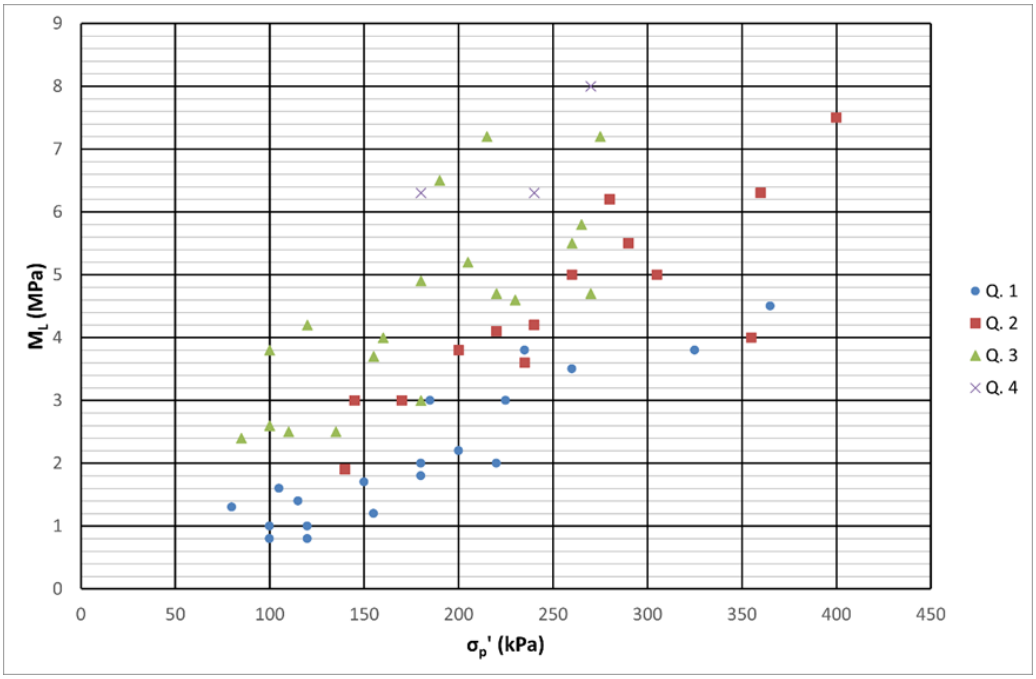

Figure 10. Interpretation of modulus M_L versus preconsolidation stress σ_p'. Q1–4 refers to the oedometer test quality according to the Karlsrud and Hernandez-Martinez [21] criterion. Figure adapted from [4].

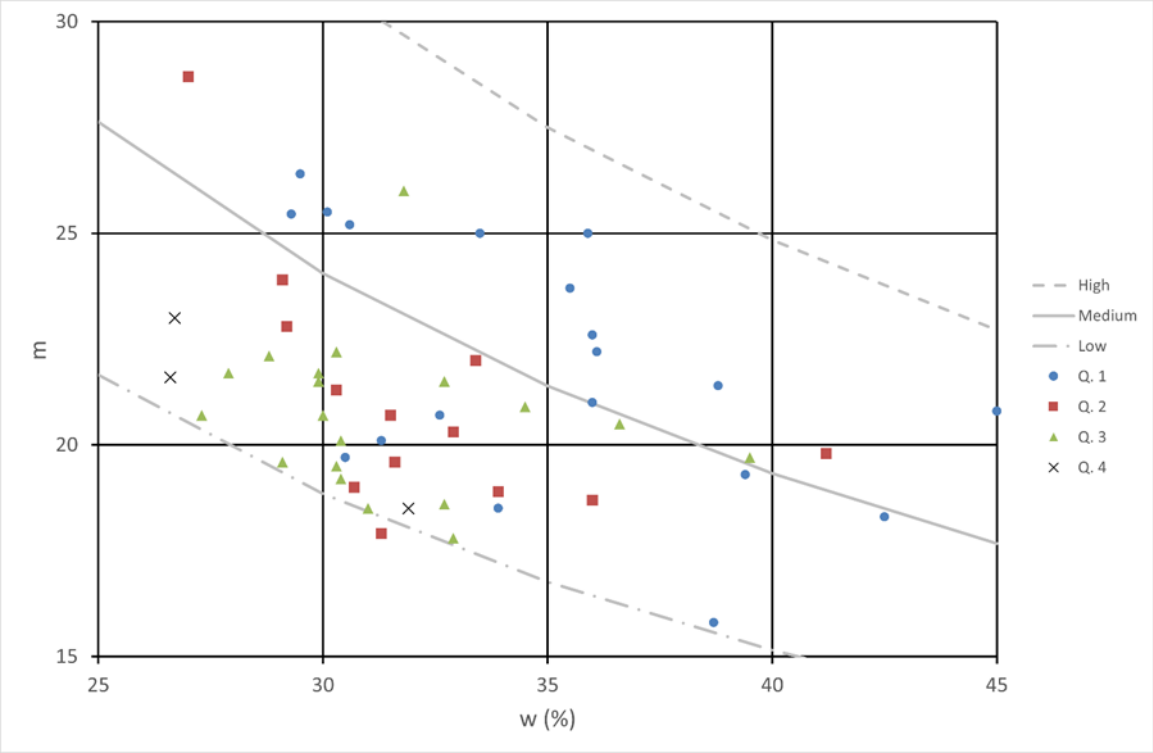

Figure 11. Interpretation of tangent modulus number m versus water content w. Q1–4 refers to the oedometer test quality according to the Karlsrud and Hernandez-Martinez [21] criterion. The plotted lines are high, medium, and low trendlines based on tests on high-quality block samples [21].

6.3. Strength

6.3.1. Undrained shear strength from triaxial tests

In triaxial tests, samples are consolidated to the best estimate of in situ stress. Vertical effective stress (σ'_v) is well-defined from the bulk density and pore pressure. Estimates of the horizontal effective stress (σ'_h) are less certain, since existing field and laboratory methods yield scattered results [35]. L'Heureux et al. [36] proposed Equation (1) for estimating the coefficient of earth pressure at rest ($K_0' = \sigma'_h/\sigma'_v$), based on regression analyses of field and laboratory data for Norwegian clays.

$$K_0' = 0.53 \cdot OCR^{0.47} \quad (1)$$

OCR interpreted from oedometer tests and CPTU was the input to the equation. $K_0' = 1.0$ was used as an upper limit. Due to practical limitations, oedometer results and pore-pressure measurements were not always available at the time the specifications of the triaxial tests were made. In these cases, assumed pore pressure and initial interpretations of CPTU were used as input in Equation (1). When oedometer and pore-pressure data were available, the undrained shear strength interpreted from the triaxial tests was corrected to account for the deviation in assumed in situ effective stresses. The proposed correction was as follows:

- The undrained shear strength was corrected linearly, with the same ratio as the deviation in the assumed effective vertical stress.

- If the estimated K_0' changed to the final interpretation, the corrected undrained shear strength was found through a geometrical construction in the MIT/NGI stress plot. Starting at the corrected initial stresses, an equal shape of the stress curve was assumed.

Figure 12 shows that the proposed corrections do not result in unreasonable changes in strength values. The correction of the undrained shear strength is between −23% and 11%. The highest and lowest plotted lines are high and low trendlines for SHANSEP parameters S and m [37], based on tests on high-quality block samples [21]. The tests performed in this project generally plot somewhere between these trendlines. The two middle lines are proposed high (S = 0.32, m = 0.73) and low (S = 0.28, m = 0.65) trendlines for the tests of quality 1–2 in this project. The proposed trendlines agree with the proposed middle trendline (S = 0.31, m = 0.70) for the NGTS quick-clay test field just south of Trondheim [19]. Figures 13 and 14 show the SHANSEP line plotted together with CPTU correlations and laboratory data at locations N11045 and N22140.

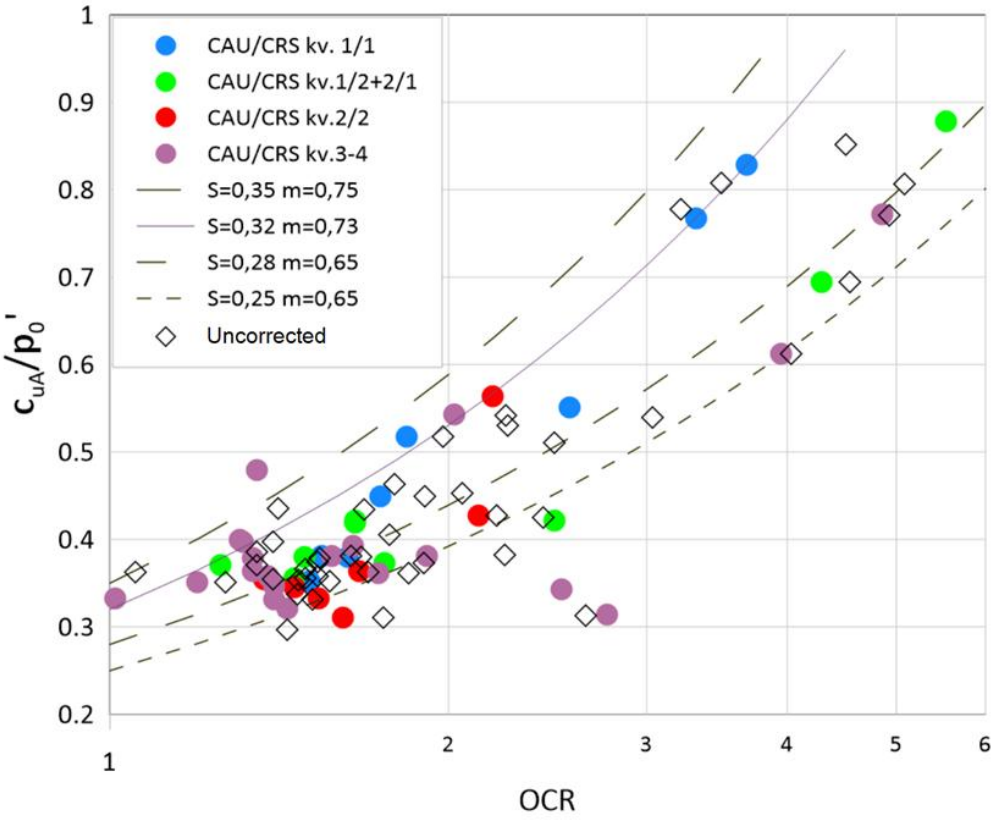

Figure 12. Normalized interpretation of undrained shear strength from triaxial tests versus OCR. Open symbols represent uncorrected strength values. Colored symbols are corrected values of different combinations of quality ("kv.") of triaxial (CAU) and oedometer (CRS) tests. The lines are based on different combinations of SHANSEP parameters. Quality according to the Karlsrud and Hernandez-Martinez [21] criterion for oedometer tests and the Lunne criterion for triaxial tests [33]. Figure adapted from [4].

To estimate the SHANSEP S parameter, four undrained triaxial tests were consolidated to stresses above the yield stress. The S parameter was calculated according to Equation (2). The tests resulted in S values in the range 0.28–0.30.

$$S = \frac{c_{uA,peak}}{\sigma'_{v\,,consolidation}} \quad (2)$$

6.3.2. Undrained shear strength from direct simple shear

Direct undrained shear strength was estimated from direct simple shear tests (DSS). The peak strength was obtained at approximately 0.75%–3% strain. To maintain strain compatibility, the interpreted direct undrained shear strength was limited to 2% strain when plotted together with other interpretations of undrained shear strength. DSS test results are plotted in Figures 13 and 14.

6.3.3. Undrained shear strength from cone penetration tests

Data from CPTU tests were used to estimate the undrained shear strength of the clay efficiently over large areas in this project. To this aim, established CPTU correlations for Norwegian clays were used (Karlsrud et al. [30] and Paniagua et al. [31]), and these were supported by advanced laboratory tests and pore-pressure measurements at some of the locations. Figures 13 and 14 show the interpretations of undrained shear strength from various field and laboratory methods. The correlations are stated below. The three correlations from Paniagua et al. [31] were among the four recommended for engineering practice. The fourth one showed more scattered interpretations [31], and was not used in this project.

$c_{uA} = \frac{\Delta u}{N_{\Delta u}} \qquad N_{\Delta u} = 6{,}9 - 4 \cdot \log OCR + 0{,}07 \cdot I_P$ (St<15)	Karlsrud et al. eq. (7a)	(3)
$N_{\Delta u} = 9{,}8 - 4{,}5 \cdot \log OCR$ (St>15)	Karlsrud et al. eq. (7b)	(4)
$c_{uA} = \frac{q_n}{N_{kt}} \qquad N_{kt} = 7{,}8 + 2{,}5 \cdot \log OCR + 0{,}082 \cdot I_P$ (St<15)	Karlsrud et al. eq. (8a)	(5)
$N_{kt} = 8{,}5 + 2{,}5 \cdot \log OCR$ (St>15)	Karlsrud et al. eq. (8b)	(6)
$c_{uA} = \frac{q_t - u_2}{N_{ke}}$		(7)
$N_{ke} = 14{,}3 - 12{,}1 \cdot B_q - 2{,}6 \cdot \log OCR + 0{,}027 \cdot I_P$	Paniagua et al. eq. (8)	

(Bq<1,0)		(8)
$N_{ke} = 6{,}4 - 3{,}3 \cdot B_q - 2{,}6 \cdot \log OCR - 0{,}015 \cdot I_P$ (Bq≥1,0)	Paniagua et al. eq. (8)	(9)
$c_{uA} = 0{,}10 \cdot q_n^{0{,}26} \cdot \Delta u^{0{,}74} \cdot w^{-0{,}26}$	Paniagua et al. eq. (1)	(10)
$c_{uA} = 0{,}32 \cdot p'_0 \cdot OCR^{(0{,}20-1{,}17 \cdot w)}$	Paniagua et al. eq. (2)	(11)

The performance of the Paniagua et al. [31] correlations was assessed in the study area. Paniagua et al.'s Eq. (1) generally yielded the highest interpreted values at locations N11045 (Holan) and N22140 (Langsteindalen Valley). The values estimated by Paniagua et al.'s Eq. (2) and Paniagua et al.'s Eq. (8) are lower and closer to the results from the triaxial tests performed on mini-block samples. Sample disturbance may cause the undrained shear strength interpreted from triaxial tests to be lower than in situ and may therefore affect which correlation fits best.

At the bottom of Langsteindalen Valley, there are several locations where CPTU correlations indicate a major reduction of the undrained shear strength just above bedrock. An example of this is at location N22140 (see Figure 14). The shear strength reduction indicated by the CPTU correlations is supported by triaxial tests. Figure 3 shows that the OCR interpreted from CPTU also reduce in this layer. Some oedometer tests performed in the area also show the same trend. One hypothesis for these effects is that the pore pressure close to bedrock is significantly higher than hydrostatic, which is plausible due to the surrounding hills. A pore-pressure sensor was installed within the layer close to bedrock to investigate this. The sensor confirmed that the pore pressure was hydrostatic also in this layer. Since the interpreted shear strength just above bedrock was not crucial to the design, this matter was not investigated further.

Figures 15 and 16 show the CPTU parameters N_{kt} and $N_{\Delta u}$ derived from tests of high quality in this project, plotted together with the average correlations from [30]. The background data for the average correlations is somewhat scattered, mostly for N_{kt}. Both the N_{kt} and $N_{\Delta u}$ values derived in this project are also scattered. However, the values derived are generally higher than the average correlations, suggesting some degree of sample disturbance. Comparing the values in this project to high-quality block samples [21], the N_{kt} values typically plot within the range of the block sample data. The $N_{\Delta u}$ values derived in this project are generally higher than the range of the block sample data (approximately 5–10).

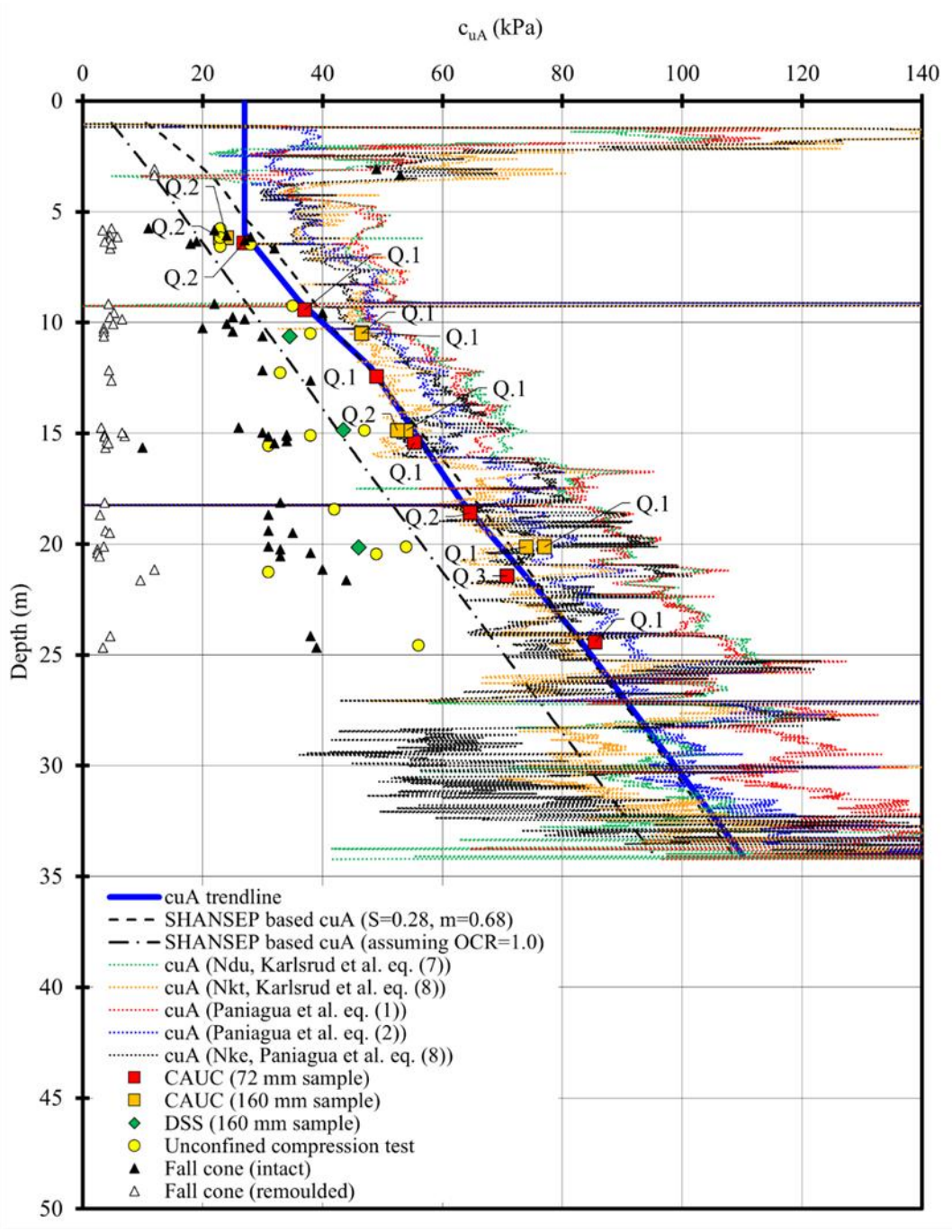

Figure 13. Undrained shear strength at Holan (location N11045) interpreted from CPTU correlations and laboratory data. Q1–Q3 refers to triaxial test quality according to the Lunne [33] criterion.

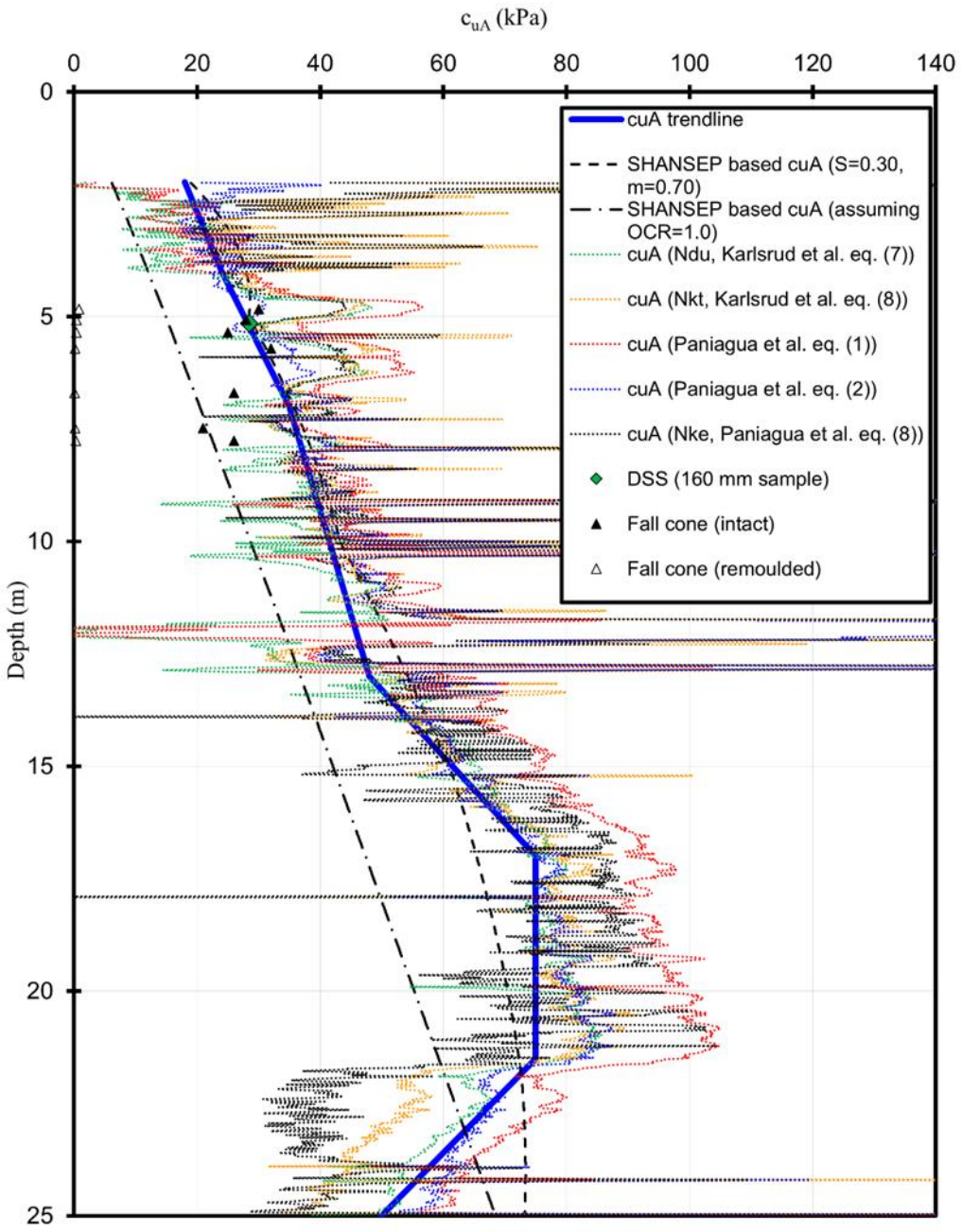

Figure 14. Undrained shear strength in Langsteindalen Valley (location N22140) interpreted from CPTU correlations and laboratory data.

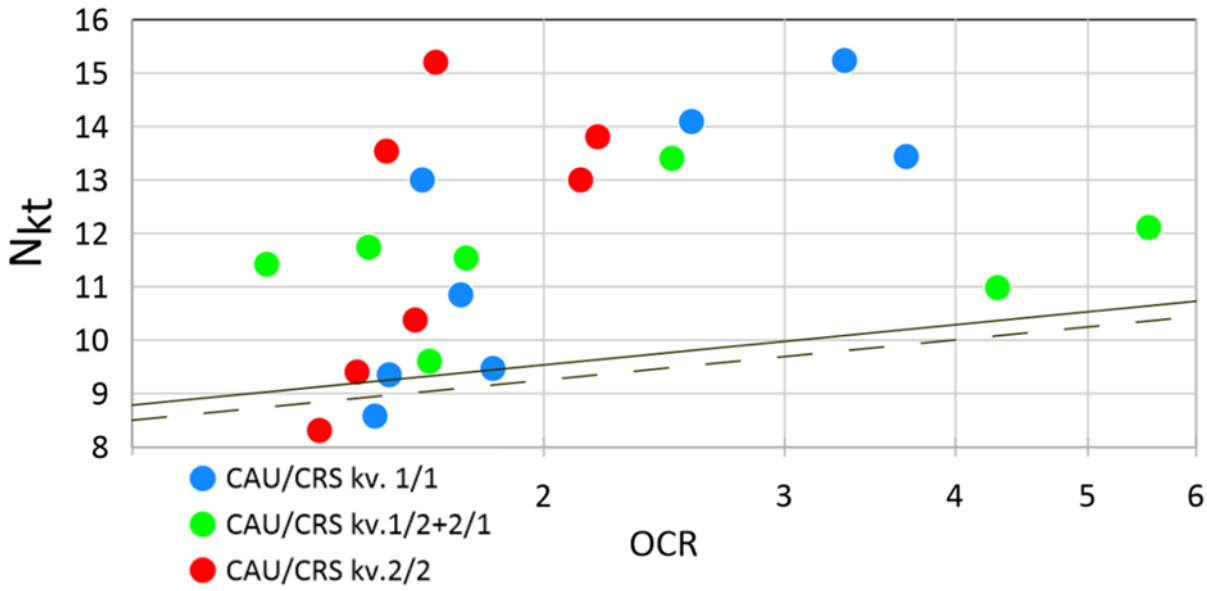

Figure 15. N_{kt} derived from tests of high quality. Correlation in [30] (equation 8) shown as a continuous line (sensitivity <15) and a dashed line (sensitivity >15), assuming a representative I_p of 12%. Quality ("kv.") according to the Karlsrud and Hernandez-Martinez [21] criterion for oedometer tests and the Lunne [33] criterion for triaxial tests. Figure adapted from [4].

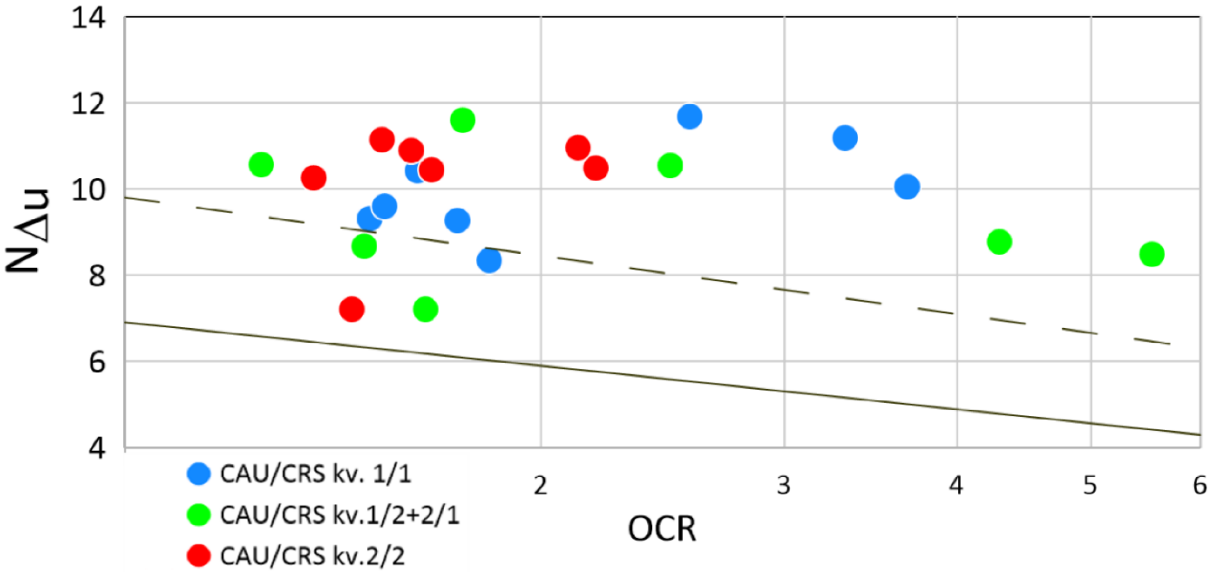

Figure 16. $N_{\Delta u}$ derived from tests of high quality. Correlation in [30] (equation 7) shown as a continuous line (sensitivity <15) and a dashed line (sensitivity >15), assuming a representative I_p of 12%. Quality ("kv.") according to the Karlsrud and Hernandez-Martinez [21] criterion for oedometer tests and the Lunne [33] criterion for triaxial tests. Figure adapted from [4].

6.3.4. Undrained shear strength anisotropy

Recommended values of anisotropy for Norwegian clays are given in [38]. The recommendations are based on the Norwegian Geotechnical Institute's (NGI) high-quality block sample database. Recommended and measured values are summarized in Table 3. The direct shear strength from DSS tests is interpreted at peak strength, hence not limited to 2% strain, as the interpretations described in chapter 6.3.2. Strength values from triaxial tests are corrected according to chapter 6.3.1.

The recommended ratio of direct to active shear strength coincides with the lower range of anisotropy measured in this project. The ratio of passive to active strength found from a single passive triaxial test is higher than the recommended ratio. It is likely that sample disturbance contributes to the scatter in the results, as well as uncertainties related to the correction of the strength interpreted from triaxial tests. Also, the number of tests is limited.

Table 3. Summary of recommended and measured anisotropy.

Ratio	Recommended ratio [38]	Measured in this project	I_p	Number of tests
c_{uD}/c_{uA}	0.63–0.66	0.6–1.0	7%–17%	4
c_{uP}/c_{uA}	0.37	0.5	16%	1

6.3.5. Effective stress strength parameters from undrained triaxial tests

Effective stress strength parameters were interpreted from plots summarizing triaxial tests from different areas and depth intervals/OCR. Figure 17 shows the interpretation for tests on samples from below 5 m depth with OCR < 3 at Holan. For samples below 5 m depth with OCR < 3 from the whole project area, a friction angle of 30° and cohesion equal to zero fits well with the data. For more shallow tests and/or OCR > 3, the best-fit friction angle increases to 33°.

6.4. Hydraulic properties

The coefficient of consolidation, c_v, varies as follows within the overconsolidated (OC) and normally consolidated (NC) parts of the oedometer tests from the whole project area:

- c_{v_OC}: 3.0–44 m^2/year
- c_{v_NC}: 1.9–14 m^2/year

Norwegian guidelines [23] state that for Norwegian clays, the coefficient of consolidation is typically in the range of 2–25 m^2/year. The interpreted values are mainly within this range but show a relatively large scatter.

The permeability k_0 is related to $c_{v,OC}$ through Equation (12). The calculated range of k_0 in this project is 2.9×10^{-10} to 3.5×10^{-9} m/s for a natural water content of 27%–39%. This is within the range of values presented in [21].

$$k_0 = \frac{c_{v,OC} * \gamma_w}{M_0} \tag{12}$$

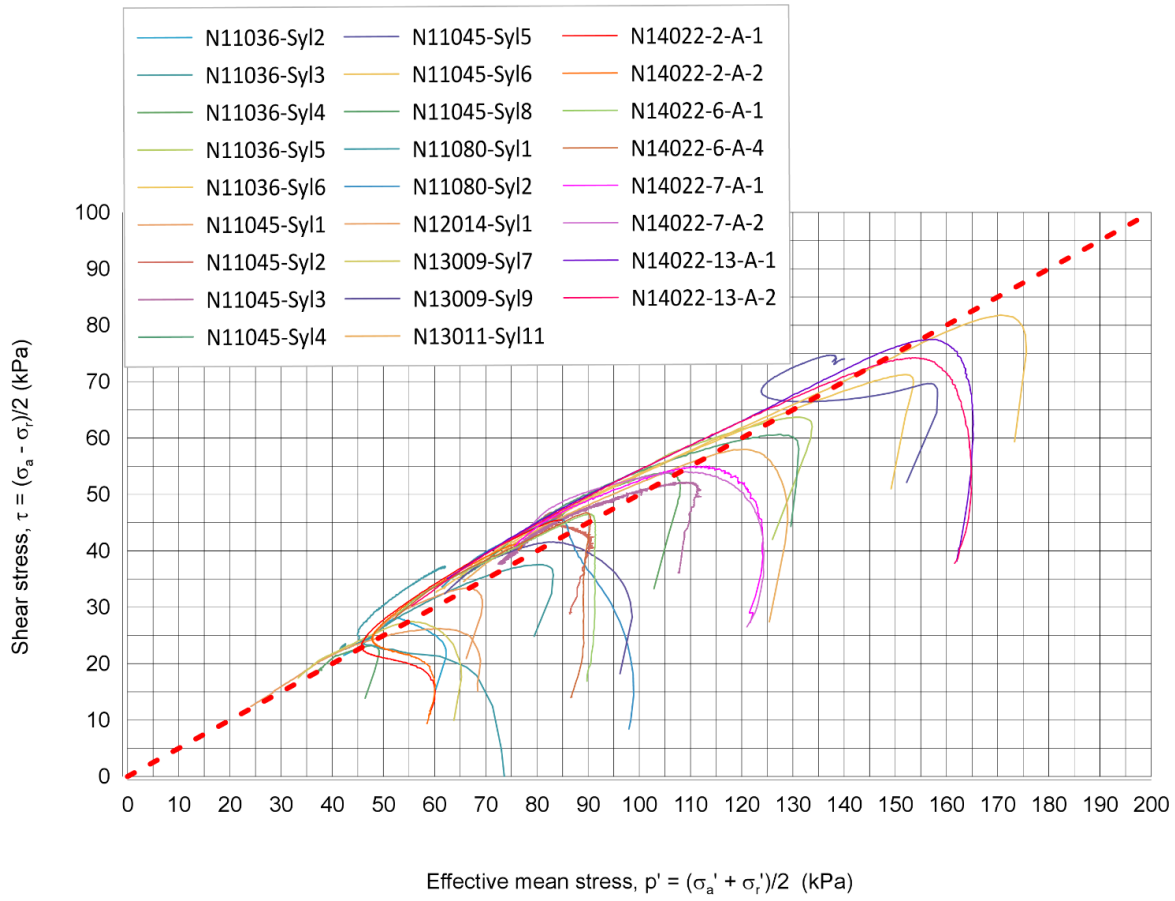

Figure 17. MIT/NGI stress plot and interpreted effective stress strength parameters (dotted red line) from undrained triaxial tests at Holan, below a 5 m depth and OCR < 3. N14022 is the name of the mini-block sampling performed at location N11045. Figure adapted from [4].

6.5. Discussion

Although the field and laboratory testing program is extensive, and many of the results seem to be of fairly good quality, it is important to emphasize that there are still uncertainties in the interpretation of characteristic values. Sample disturbance will still play an important role, and in addition, there are uncertainties connected to correlations, pore pressures, and situ stresses, especially in layered ground, and testing procedures in the laboratory. Interpretation of CPTUs and the choice of consolidation stresses in advanced laboratory testing generally assumes a horizontal ground surface and a vertical major principal stress. This might deviate considerably from the in situ stresses in naturally sloping ground. In addition, in situ shear rate, temperature, and strain conditions deviate from laboratory conditions. Undrained triaxial tests at NGI are, by default, done at a deformation rate of 1.4% per hour, which would typically be higher than actual in situ strains. Tests at a slower rate show strengths down to

about 80% of normal laboratory rates [39]. Laboratory tests are done at a temperature of 20 °C, while ground temperature in Norway is about 4–6 °C, typically leading to an underestimation of preconsolidation stress and strength [39]. The intermediate principal stress will be lower in laboratory tests than experienced in the field, leading to an underestimation of average effective stress. The accumulated effect of all these shortcomings is generally assumed to give a conservative estimation of strength, which can lead to unrealistic calculation results in, e.g., stability calculations. If the safety factor is lower than unity, the strength can be increased to obtain equilibrium. However, caution should be taken when extrapolating this correction into new stress conditions, as it is not obvious to which aspect the error is attributed.

7. Large-scale field tests

7.1. Lime-cement soil stabilization test field

Ground improvement was necessary for many of the highway embankments. During design, the aim was to maximize the use of prefabricated vertical drains (PVD), supplemented with lime-cement columns where the increased strength from consolidation was not sufficient to meet the required level of safety. This approach was used to limit carbon dioxide emissions and negative environmental impact as much as possible. The optimal quantity of binder to reach the desired design shear strength of 250 kPa for the lime-cement columns was established based on the results from large-scale field tests. The large-scale field tests also focused on the following aspects:

- Comparison of strength development for two binders available in the region: a mixture of 50% cement and 50% quicklime, and a mixture of 50% cement and 50% cement kiln dust (CKD).
- Investigating the anisotropy of deep mixed clay.
- Investigating the verticality of the deep mixed columns.

The first point aimed to give the client a basis for choosing the type of binder, considering both technical and economic aspects. Strength anisotropy and verticality are also important issues for design that were investigated in the field.

Figure 18 presents mean strength estimates from a series of column penetration (KPS) tests on the lime-cement mixture and cement-cement kiln dust mixture [40]. The two binders gave very similar shear strength results, increasing from ca. 200 kPa below the working platform to ca. 700–800 kPa at a depth of 10 m, after 22 days of curing. The strength below 10 m depth decreased somewhat, but a large part of this can be explained by some of the penetration tests exiting the columns and thus decreasing the mean value. This is therefore not related to varying soil conditions or a decreased column strength. The overall results, however, showed that the two binders gave similar strength and variability in terms of coefficient of variation, giving the client the flexibility to choose binder type based on cost and availability. The client opted for the lime-cement binder type due to lower cost.

Figure 19 shows results from a series of active and passive triaxial tests on samples taken from deep mixed columns in the field [41]. Two types of passive triaxial tests were performed: extension tests with constant axial stress and increasing radial stress (TE tests), and tension tests with decreasing axial stress and constant radial stress (TT tests). The results indicated that the effective strength parameters are isotropic; however, there is an anisotropy for maximum shear strength (the term "undrained strength" should not be used for a lime-cement column, which probably behaves partly

drained upon loading). The ratio of passive to active maximum shear strength was between 0.45 and 0.95, with an average of 0.67. This had important consequences for design, and a lower shear strength was thus used when the columns were placed in the passive zone, i.e., at the toe of the embankments.

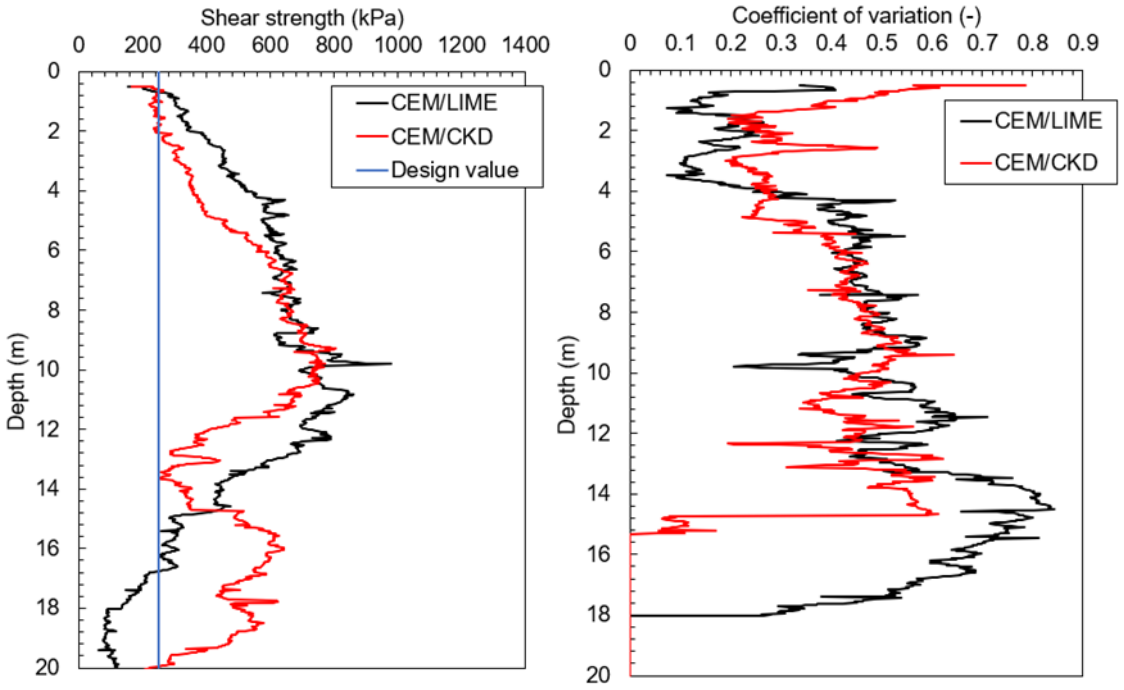

Figure 18. Results from KPS tests using two different binders: a) strength; b) coefficient of variation.

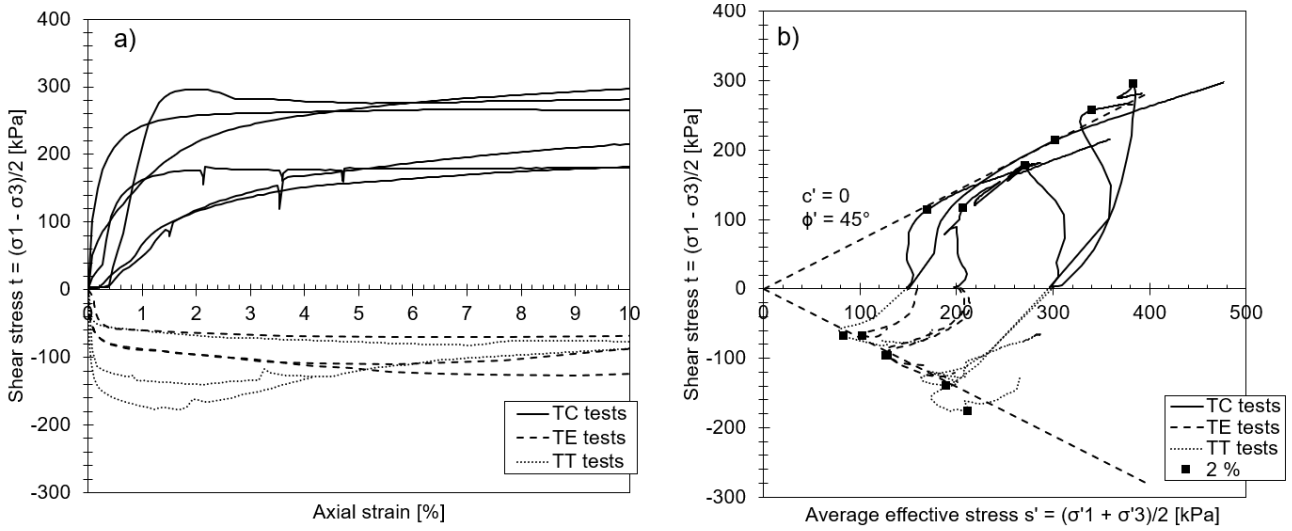

Figure 19. Results from isotropically consolidated undrained triaxial tests: a) stress-strain plot; b) effective stress paths in the MIT plot. TC = triaxial compression, TE = triaxial extension, TT = triaxial tension.

Verticality measurements were performed with a high-accuracy gyroscope-inclination sensor, DeviGyro RG30 Slimline [42], manufactured by Devico Norway. Measurements were performed in

10 columns placed in a single shear panel and 20 columns placed in a double shear panel, with the purpose of investigating if there were any differences in verticality and hence overlap between columns in the single and double panels. Figure 20 shows the measured column locations at 15 m depth [43]. Several parts of the shear panels lacked overlap, with no significant difference between the single and double shear panels, allowing the design to be made with single panels, which are slightly more efficient in terms of area coverage ratio. How this partial lack of overlap affects the global behavior of an embankment on lime-cement improved ground in shear panels needs to be investigated further. Nevertheless, it shows one limitation of the lime-cement method and clearly shows the need for a conservative approach when used for stability purposes, especially when improving deep clay deposits.

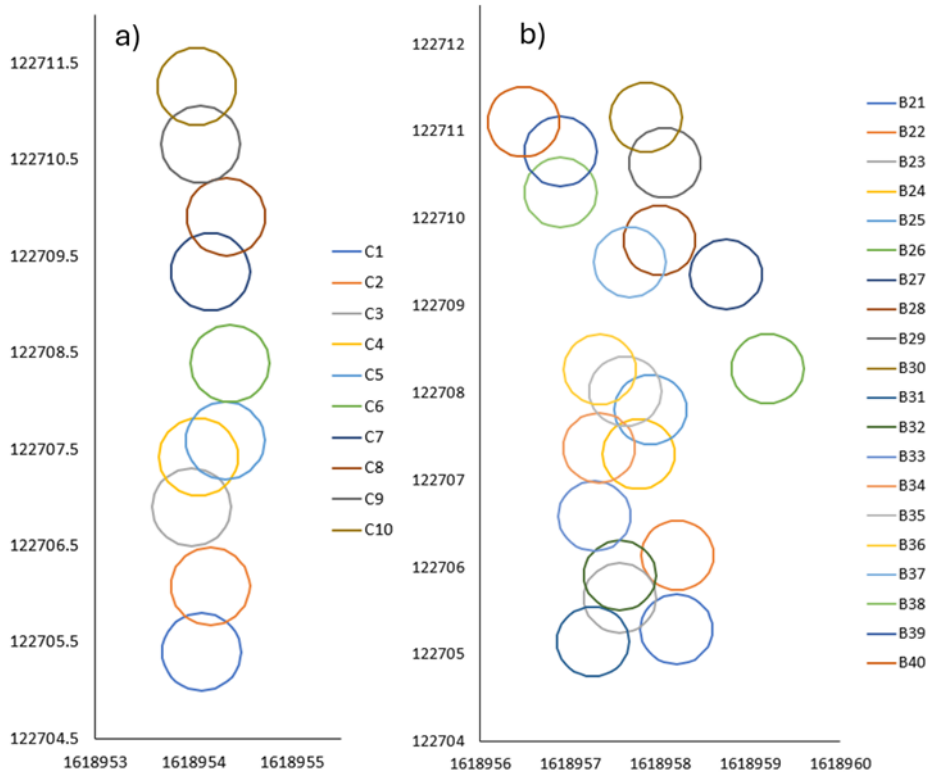

Figure 20. Location of columns at 15 m depth based on data from the verticality measurements: a) single shear panel; b) double shear panel.

7.2. Embankment on soft soil at Holan

At Holan, a 400 m long road bridge is founded on steel core piles down to bedrock and connected to a 7 m high embankment on original ground. Figure 21 shows the 3D model from the design phase and a cross-section with the permanent terrain and the preloading fill. To achieve acceptable differential settlements between the abutment (with negligible settlements) and the embankment, vertical drains in combination with preloading were used. As a supplement, lime cement columns were also installed in a belt close to the creek and the abutment for both stability and settlement purposes. The center distance of the vertical drains was determined to ensure almost full consolidation of the clay during the construction phase. To correctly assess the stability of the slopes toward the creek and

to minimize ground reinforcement using lime-cement in this project, the shear strength of the clay below the embankment was gradually increased in the analysis to account for consolidation. Soil layering along a profile at Holan is shown in Figure 21.

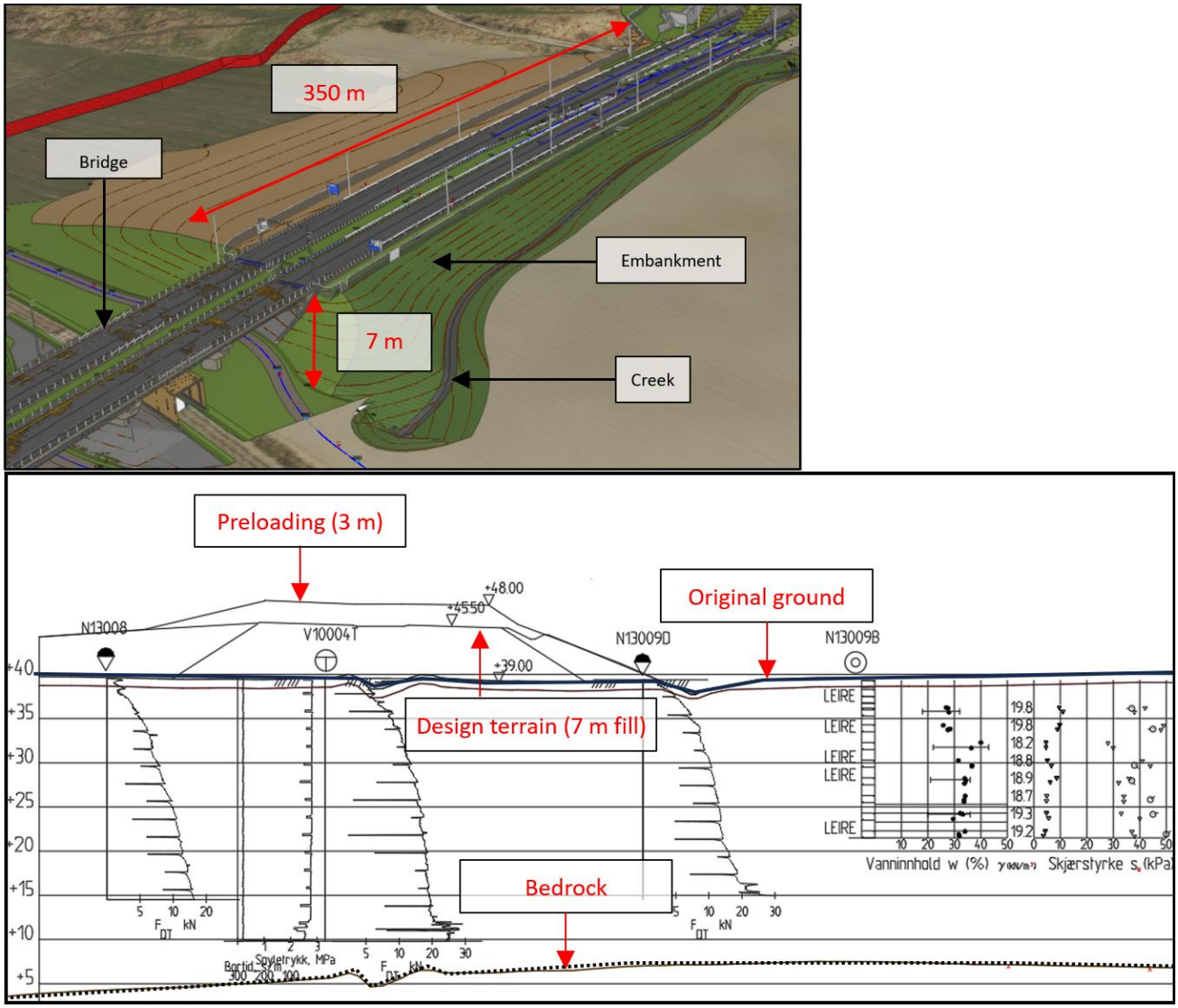

Figure 21. Top: Designed 3D model of the bridge and the embankment at Holan. Bottom: Cross-section with soil profile, permanent terrain, and preloading.

During the construction phase, pore-pressure measurements were used to control the filling rate, ensuring sufficient stability at all times. Measured pore-pressure dissipation agreed very well with theoretical curves from the design (Figure 22). The dotted lines in the figure represent predictions of pore-pressure dissipation for vertical drains with a center distance of 1.0 and 1.5 m. The installed center distance of the vertical drains was 1.2 m. With this solution, it was possible to minimize the extent of lime-cement columns and, at the same time, achieve acceptable differential settlements. The design methodology is presented in detail in Amdal et al. [44].

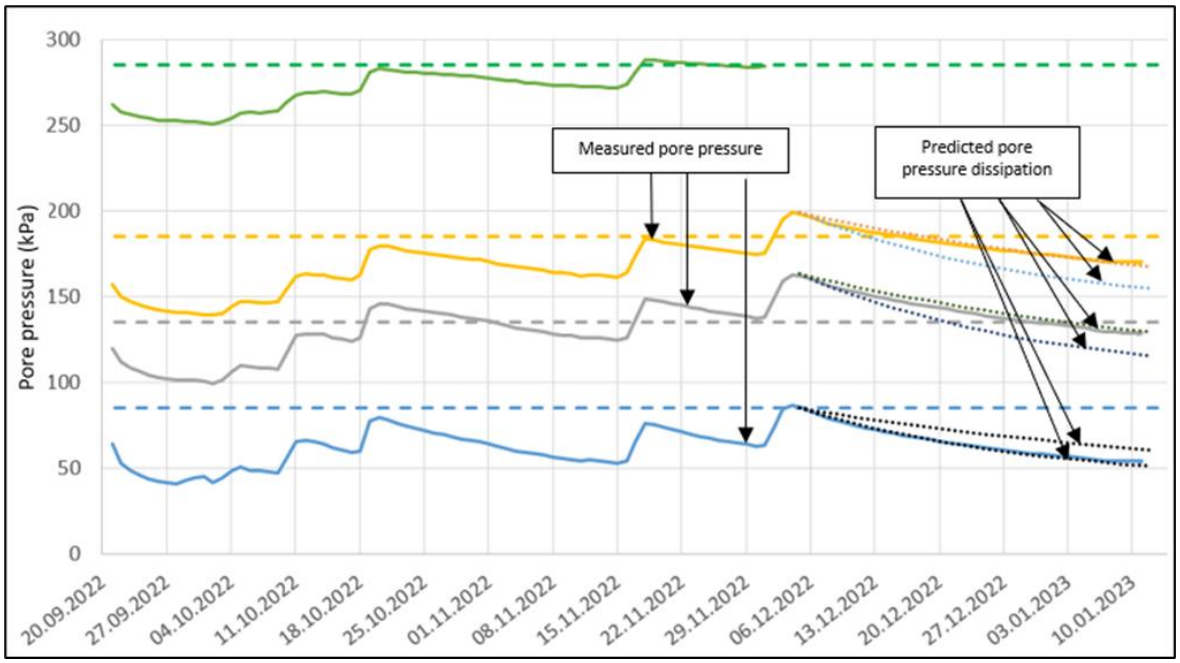

Figure 22. Measured pore pressures during the construction phase. The black dotted lines represent predicted dissipation curves from the design. The piezometers were installed at 5, 10, 15, and 25 m depth.

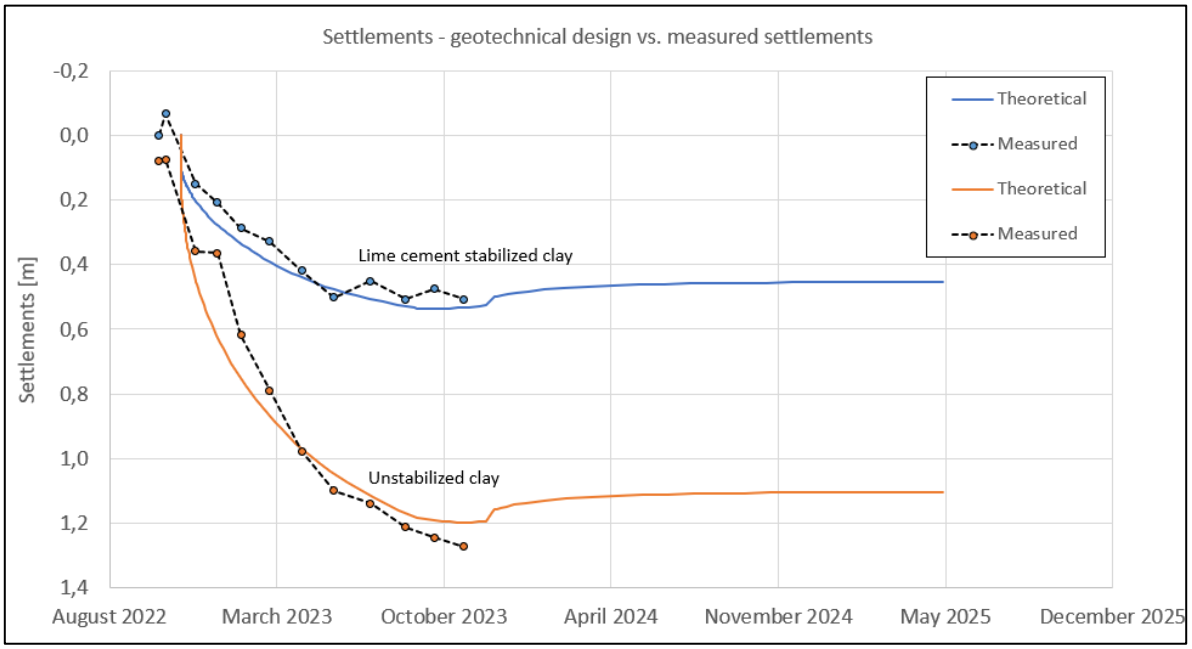

Figure 23. Settlement time series, measured vs. calculated settlements from design phase at Holan. The blue lines represent an area with lime cement columns (single pattern), and the orange lines represent an area without lime cement columns.

Settlements at Holan were monitored using a Consoil hydrostatic profiler [45]. Figure 23 shows the measured and calculated settlement for two different sections; the blue curve represents an area

where the clay is stabilized with single lime cement columns, and the orange curve represents an area where the clay is not stabilized. There is a good match between the measured settlements and the settlements presented in the early design phase. It should be mentioned that the actual preloading was larger than in the design phase (the preloading from the design phase was 3 m, but in practice it was 4 m). This was mostly due to practical reasons (for storing more mass). After the preloading was removed in early 2024, data collection was stopped. The maximum measured settlement was 130 cm. Assuming a maximum embankment height of 11 m and a clay thickness of 35 m, the average oedometer modulus for the clay is back-calculated to 6 MPa.

7.3. Embankment on soft soil in the Langsteindalen Valley

Further north, in Langsteindalen Valley, the road embankment was constructed to a height of 14 m on the original ground. Here, the foundation soil consists of ca. 40 m of sensitive clay over bedrock. As for Holan, vertical drains in combination with 2 m preloading were used to accelerate the settlement rate and to achieve acceptable settlement rates at the time of completion. The settlements were monitored using settlement plates every 50 m along the road (Figure 24). The settlements were measured every 2 weeks during the construction phase and after the preloading was removed, resulting in about 2 years of settlement data.

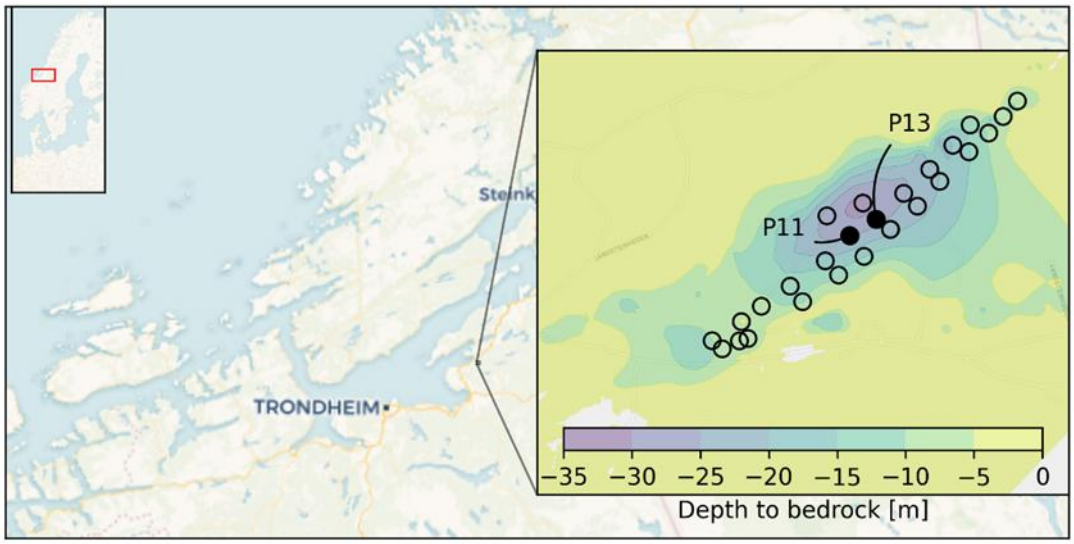

Figure 24. Location of sensors P11 and P13 marked for measurements of settlements in Langsteindalen Valley. The sensors are shown on a contour map of depths to bedrock [46].

The Norwegian Public Roads Administration (NPRA) requires that the road does not exceed 40 cm of total settlements within 40 years after construction. The aim of the geotechnical design was to allow for primary consolidation to be finished during the construction period.

Settlement data were used to predict the total settlements and to document that the requirements for the remaining settlements are likely to be met in the operation phase. Sensor P13, which was located in the area where vertical drains had been installed, showed the largest settlement development and was therefore considered in this paper. Using regression analysis and probabilistic models (presented in Nøst

et al. [46]), the remaining settlements were forecasted. Figure 25 shows the historic measurements in combination with the predicted settlements for sensor P13. The last measured settlement in late 2024 is 118 cm. The mean predicted final settlement is 123 cm (at infinity), and settlement values within 95% prediction interval are between 120 and 128 cm. The requirement of a maximum of 40 cm of settlements after 40 years of operation is therefore met within a 95% probability interval.

Using Asaoka's method, it is possible to back-calculate the consolidation coefficient c_v for the clay, including the effect of vertical drains, based on the measured settlement values. For the settlement time-series for sensor P13, the calculated c_v is 260 m^2/year. This value is about 10–100 times larger than the values obtained from laboratory tests on clay, without the effect of vertical drains (see chapter 6.4).

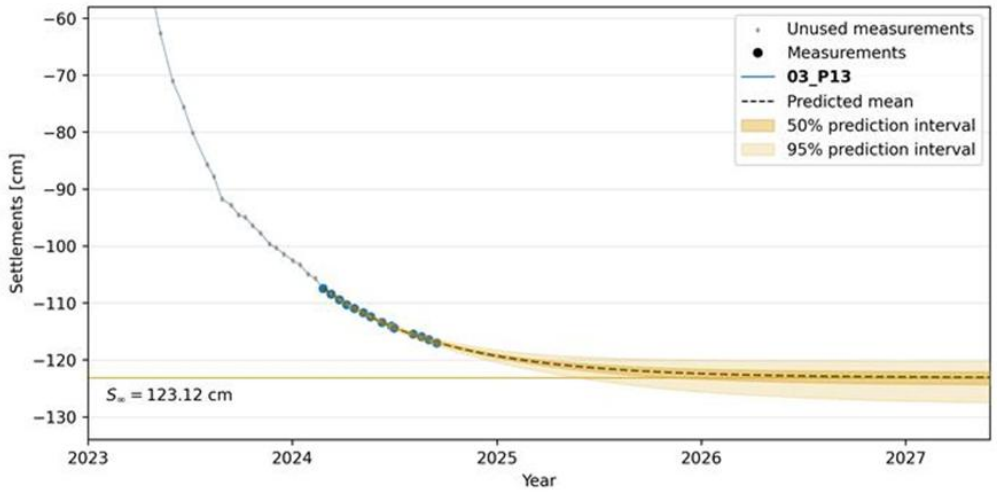

Figure 25. Settlement predictions for sensor P13 for the embankment in Langsteindalen Valley.

8. Summary and conclusions

The properties of vast and sensitive clay deposits have been investigated for the construction of the E6 Kvithammar-Åsen highway in mid-Norway. Airborne electromagnetic scanning enabled efficient optimization of the field investigation program, which included a large number of total and rotary pressure soundings, CPTU, piezometers, and undisturbed sampling.

The state, index, and engineering properties of the clay deposits were characterized. The performance of several correlations for OCR and undrained shear strength from CPTU have been evaluated. Data from this highway construction project is compared to reference data from the nearby test site at Tiller-Flotten and the high-quality Norwegian block sample database of NGI. The advanced laboratory tests indicate that higher-quality samples are obtained from larger diameter samplers. Sample disturbance is a key uncertainty for the results presented in this article.

The key outcomes of large-scale testing of lime-cement stabilization and road embankments on soft ground have been presented.

Author contributions

Anders Lindgård: Conceptualization, Methodology, Formal analysis, Investigation, Data

Curation, Writing – Original draft, Writing – Review & Editing, Visualization, Project Administration. Vidar Gjelsvik: Conceptualization, Methodology, Formal analysis, Investigation, Data Curation, Writing – Original draft, Writing – Review & Editing, Visualization, Supervision. Åse Marit Wist Amdal: Conceptualization, Methodology, Formal analysis, Investigation, Data Curation, Writing – Original draft, Writing – Review & Editing, Visualization, Project administration. Sølve Hov: Conceptualization, Methodology, Formal analysis, Investigation, Data Curation, Writing – Original draft, Writing – Review & Editing, Visualization, Supervision. Jean-Sébastien L'Heureux: Conceptualization, Methodology, Writing – Original draft, Writing – Review & Editing, Supervision. Katharina Kahrs: Formal analysis, Investigation, Data Curation, Writing – Review & Editing. Sigbjørn Rønning: Conceptualization, Methodology, Investigation, Writing – Review & Editing, Supervision, Funding Aquisition.

Use of AI tools declaration

The authors declare they have not used Artificial Intelligence (AI) tools in the creation of this article.

Acknowledgments

Preparation of the article was supported by the basic funding to NGI from The Research Council of Norway. Data was provided through work on the project together with Nye Veier as project owner and Hæhre Entreprenør as contractor.

Conflict of interest

All authors declare no conflicts of interest in this paper.

References

1. Lacasse S (2013) 8th Terzaghi Oration Protecting society from landslides–the role of the geotechnical engineer, *Proceedings of the 18th international conference on soil mechanics and geotechnical engineering*, Paris, 15–34.
2. Gregersen O (1981) *The quick clay landslide in Rissa, Norway*, Norwegian Geotechnical Institute Publication, 135: 1–6.
3. Solberg IL, Long M, Baranwal VC, et al. (2016) Geophysical and geotechnical studies of geology and sediment properties at a quick-clay landslide site at Esp, Trondheim, Norway. *Eng Geol* 208: 214–230. https://doi.org/10.1016/j.enggeo.2016.04.031
4. Norwegian Geotechnical Institute, 20180628-12-R R1-GEOT-08 Tolkning av geotekniske parametere, Stjørdal, rev. 03. 2021.
5. Long M, Heureux J-S, Bache BKF, et al. (2019) Site characterisation and some examples from large scale testing at the Klett quick clay research site. *AIMS Geosci* 5: 344–389. https://doi.org/10.3934/geosci.2019.3.344

6. L'Heureux J-S, Lunne T (2020) Characterization and Engineering properties of Natural Soils used for Geotesting. *AIMS Geosci* 6: 35–53. https://doi.org/10.3934/geosci.2020004
7. NGU, Løsmasser—Nasjonal løsmassedatabase, 2024. Available from: https://geo.ngu.no/kart/losmasse_mobil/.
8. Kartverket, Norgeskart, 2024. Available from: https://norgeskart.no/.
9. Christensen C, Skurdal G, Pfaffhuber A, et al. (2020) Airborne geoscanning and efficient geotechnical ground investigation workflows: A road-building case study from Central Norway, Helsinki, Finland, 25–27.
10. Norsk geoteknisk forening (NGF), Melding nr. 9 rev. 1 Veiledning for utførelse av totalsondering, 2018. Available from: https://ngf.no/wp-content/uploads/2020/02/NGF-Melding-9-Totalsondering-Rev-1-2018.pdf.
11. Norsk geoteknisk forening (NGF), Melding nr. 7 rev. 1 Veiledning for utførelse av dreietrykksondering, 1989. Available from: https://ngf.no/wp-content/uploads/2015/03/7_NGFMelding07.pdf.
12. Lunne T, Powell JJ, Robertson PK (2002) *Cone penetration testing in geotechnical practice*, CRC Press. https://doi.org/10.1201/9781482295047
13. Norwegian Geotechnical Institute, 20180628-06-R R1-GEOT-02 Datarapport grunnundersøkelser Holvegen og E6 Stjørdal, rev. 5. 2024.
14. Norsk geoteknisk forening (NGF), Melding nr. 5 rev. 3 Veiledning for utførelse av trykksondering, 2010. Available from: https://ngf.no/wp-content/uploads/2015/03/5_NGF-Melding-5-CPTU-_revisjon-3.pdf.
15. Norsk geoteknisk forening (NGF), Melding nr. 6 rev. 2 Veiledning for måling av grunnvannsstand og poretrykk, 2017. Available from: https://ngf.no/wp-content/uploads/2015/03/NGF-melding-6-Poretrykksmaling-2017.pdf.
16. Norsk geoteknisk forening (NGF), Melding nr. 11 Veiledning for prøvetaking, 2013. Available from: https://ngf.no/wp-content/uploads/2015/03/NGF-Melding-11-Provetaking-2014.pdf.
17. Emdal A, Gylland A, Amundsen HA, et al. (2016) Mini-block sampler. *Can Geotech J* 53: 1235–1245. https://doi.org/10.1139/cgj-2015-0628
18. Reite AJ, Misund A, Banks D, et al. (1994) Weichselian and Holocene geology of Sør-Trøndelag and adjacent parts of Nord-Trøndelag county, Central Norway.
19. L'Heureux JS, Lindgård A, Emdal A (2019) The Tiller-Flotten research site: Geotechnical characterization of a sensitive clay deposit. *AIMS Geosci* 5: 831–867. https://doi.org/10.3934/geosci.2019.4.831
20. Rosenqvist IT (1953) Considerations on the sensitivity of Norwegian quick-clays. *Geotechnique* 3: 195–200. https://doi.org/10.1680/geot.1953.3.5.195
21. Karlsrud K, Hernandez-Martinez FG (2013) Strength and deformation properties of Norwegian clays from laboratory tests on high-quality block samples. *Can Geotech J* 50: 1273–1293. https://doi.org/10.1139/cgj-2013-0298
22. Moum J (1965) Falling drop used for grain-size analysis of fine-grained materials. *Sedimentology* 5: 343–347. https://doi.org/10.1111/j.1365-3091.1965.tb01566.x
23. Norsk geoteknisk forening (NGF), Melding nr. 2 rev. 2 Veiledning for symboler og definisjoner i geoteknikk, 2011. Available from: https://ngf.no/publikasjoner/melding-nr-2-veiledning-for-symboler-og-definisjoner-i-geoteknikk-1982/.

24. Standard Norge, NS-EN ISO 14688-2:2018 Geotechnical investigation and testing—Identification and classification of soil - Part 2: Principles for a classification (ISO 14688-2:2017), 2018. Available from: https://online.standard.no/nb/ns-en-iso-14688-2-2018.
25. Sandven R, Montafia A, Gylland AS, et al. (2015) NIFS Rapport nr. 126/2015. Detektering av kvikkleire—Sluttrapport, 2015. Available from: https://publikasjoner.nve.no/rapport/2015/rapport2015_126.pdf.
26. Leroueil S, Tavenas F, Samson L, et al. (1983) Preconsolidation pressure of Champlain clays. Part II. Laboratory determination. *Can Geotech J* 20: 803–816. https://doi.org/10.1139/t83-084
27. Standard Norge, NS 8015:1988 Geoteknisk prøving—Laboratoriemetoder—Bestemmelser av udrenert skjærstyrke ved konusprøving, 1988. Available from: https://online.standard.no/nb/ns-8015-1988.
28. Sandven R, Vik A, Rønning S, et al. (2012) NIFS Rapport nr. 46/2012. Detektering av kvikkleire fra ulike sonderingsmetoder. Available from: https://publikasjoner.nve.no/rapport/2012/rapport2012_46.pdf.
29. Norsk geoteknisk forening (NGF), Melding nr. 12 Veiledning for detektering av sprøbruddmateriale, 2019. Available from: https://ngf.no/wp-content/uploads/2020/02/NGF-melding-12-Veiledning-for-detektering-av-sprobruddmateriale.pdf.
30. Karlsrud K, Lunne T, Kort DA, et al. (2005) *CPTU correlations for clays*, AA BALKEMA PUBLISHERS, 693.
31. Paniagua P, D'Ignazio M, L'Heureux J-S, et al. (2019) CPTU correlations for Norwegian clays: an update. *AIMS Geosci* 5: 82–103. https://doi.org/10.3934/geosci.2019.2.82
32. Mayne PW (1986) CPT indexing of in situ OCR in clays. *Use of In Situ Tests in Geotechnical Engineering*, ASCE, 780–793.
33. Lunne T, Berre T, Strandvik S (1997) Sample disturbance effects in soft low plastic Norwegian clay. *Symposium on Recent Developments in Soil and Pavement Mechanics*, Rio de Janeiro, Brazil, 81–102.
34. Berre T, Lunne T, L'Heureux J-S (2022) Quantification of sample disturbance for soft, lightly overconsolidated, sensitive clay samples. *Can Geotech J* 59: 300–303. https://doi.org/10.1139/cgj-2020-0551
35. Ofstad CS, Lindgård A (2017) Field and Laboratory Investigations to Evaluate the Coefficient of Earth Pressure at Rest-NGTS Flotten Quick Clay Test Site, Master's thesis, NTNU.
36. L'Heureux J-S, Ozkul Z, Lacasse S, et al. (2017) A revised look at the coefficient of earth pressure at rest for Norwegian Clays. Norwegian Geotechnical Society (NGF), Oslo, Norway.
37. Ladd CC, Foott R (1974) New design procedure for stability of soft clays. *J Geotech Geoenviron Eng* 100. https://doi.org/10.1061/AJGEB6.0000066
38. Thakur V, Oset F, Viklund M, et al. (2014) NIFS-rapport nr. 14/2014. En omforent anbefaling for bruk av anisotropifaktorer i prosjektering i norske leirer, NVE.
39. Lunne T, Andersen KH (2007) Soft Clay Shear Strength Parameters For Deepwater Geotechnical Design, *Proceedings of the 6th International Offshore Site Investigation and Geotechnics Conference: Confronting New Challenges and Sharing Knowledge*, London, UK.
40. Norsk geoteknisk forening (NGF), Recommendations for ground improvement with lime-cement columns, 2012. In Norwegian.

41. Hov S, Paniagua P, Karlsrud K (2024) A Study of the Anisotropy of Improved Clay Using the Nordic Dry Deep Mixing Method, Hanoi, In: Duc Long, P, Dung NT, Eds., *Proceedings of the 5th International Conference on Geotechnics for Sustainable Infrastructure Development*, 395: 1113–1123. Springer, Singapore. https://doi.org/10.1007/978-981-99-9722-0_73.
42. Devico, DeviGyro RG30 SLIMLINE, 2024. Available from: https://www.devico.com/product/devigyro/devigyro-rg30/.
43. Hov S, Berner MN, Rønning S, et al. (2024) Strength and Verticality of Nordic Dry Deep Mixing Columns—A Case Study in Norway, In: Duc Long P, Dung NT, Eds., *Proceedings of the 5th International Conference on Geotechnics for Sustainable Infrastructure Development*, 395: 1051–1066. Springer, Singapore. https://doi.org/10.1007/978-981-99-9722-0_69
44. Amdal ÅMW, Hov S (2023) E6 Kvithammar—Åsen: Embankment on clay in combination with vertical drains and preloading, Oslo, Norway.
45. Consoil Consoil Hydrostatic Profiler. Available from: https://hmagrp.com/consoil-hydrostatic-profiler/.
46. Nøst HA, Amdal ÅMW, Tsegaye AB, et al. (2025) Predicting settlements development under road embankment using Probabilistic models, Oslo, Norway, In press.

AIMS Press